April 2018

Functionally-Graded Soft Robotic Actuators

Adam B. White
Worcester Polytechnic Institute

Jiacheng Liu
Worcester Polytechnic Institute

Reynaldo David Duran
Worcester Polytechnic Institute

Steven H. Rangel
Worcester Polytechnic Institute

Functionally-Graded Soft Robotic Actuator

A Major Qualifying Project
Submitted to the Faculty
of the
WORCESTER POLYTECHNIC INSTITUTE
by

Reynaldo Duran
Jiacheng Liu
Steven Rangel
Adam White

Date: April 26, 2018

Submitted to:
Professor Nima Rahbar
Professor Cagdas Onal

Contents

1. Abstract

The goal of this project is to design, analyze, and fabricate a pneumatically powered, functionally-graded soft robotic actuator made of a polymer embedded with nanoparticles, and later attach three of them into a hand-sized, remotely-controlled gripper assembly for object distribution. This was accomplished through 3D modeling, finite element analysis, polymer-nanoparticle mix tensile testing, and construction of a mechatronic arm controlled by a wearable gesture controller. Results show that the functionally-graded actuator produces 1.6 times the lateral force output and twice the displacement than the 15wt% control actuator.

2. Introduction

2.1. Soft Robotics

Soft robotics is the subfield of robotics that deals with robots composed of highly compliant, soft, flexible materials (as opposed to the usual rigid joints), often mimicking the physical properties of living organisms, much like elephant trunks or octopus arms. They are good at simulating natural movements and are often used to act as artificial muscles [1]. Soft robots can mimic living muscle through fluid changes in shape and size. With many applications, soft robotics has potential for use in fields like biomedical engineering, biomechanics, mathematical modeling, biopolymer chemistry, computer science, and tissue engineering. Another draw to soft robotics as an emerging field is its low costs and shallow learning curves, relative to other subsets of robotics. A soft robot can be built with essentially just machined or printed molds, a liquid polymer, and a simple control system [2]. Fluidic elastomer actuators are a group of soft actuators that consist of low-durometer rubbers and are pressurized with low-pressure fluid, usually within the range of 3 to 8 psi.

2.2. Current Shortcomings

Opportunities in soft robotics research include the exploration of unconventional materials and their implementation in robotic systems. Researchers seek to understand the interactions between soft robots and their complex environments because it is vital for sys-

tematic development of technologies and theories of emergent adaptive behaviors [3]. A challenge that comes along with this is representing the state variables of body posture for soft robotic systems because the dimensions of design parameters are dramatically changing depending on the postures. This was a simpler task when dealing with rigid components, but introducing the continuous mechanical deformation property makes kinematic analysis of soft robots far more complicated. Beyond this, researchers are striving to make actuators and sensors smaller, softer, and more deformable. Microfabrication technologies show potential for fully embedded actuation and for feedback and controllability of the actuator. Strong advantages to soft robots is their silent operation, portability, quick and inexpensive fabrication, and inherent safety. These are features that should be maximized to achieve full potential of this technology [26]. Looking forward, the challenge for soft robotics lies in becoming a universally accessible and inexpensive tool through designing, integrating, interfacing, and controlling flexible materials so that they can perform real-world tasks [6].

2.3. Applications

Robots, in general, are made to be efficient, precise, strong and stiff in order to accomplish tasks effectively, and using less effort than humans. And now, with the breakthrough of soft robotic technology, many exciting tasks that could never have been done by rigid-body robots are now achievable. Soft robotics is playing significant roles in applications such as healthcare, animal studies, food processing, and beyond. Soft robots are needed for safe interaction with living organisms within natural or human-built environments. More specifically, their use can be applied in minimally-invasive surgery, assistive healthcare devices, emergency search-and-rescue situations, instrument repair, mine detection, and more [4].

Most animals have soft bodies, which cannot be modeled by traditional robots. In order to study how animals use their neuromechanical control system to govern their body movements, soft robots allow scientists to build, visualize and discover more about the

brilliant mechanical designs of animals [5]. Reliance on soft material properties is a key to how natural organisms operate differently from robots. Animals leverage softness to overcome the limitations in their imperfect knowledge of their environment, slow processing speeds, and relative imprecision [6]. Soft robotics is also a great innovation for the food and agriculture industries, especially for automation farms and food packaging firms. The metallic gripper is not commonly used in these fields due to its hard material properties, which can easily cause damage to products. Soft grippers are currently the main product, as its fluidic and adaptable mechanisms are great for picking fragile foods like eggs and fruits, for example. Shapes of fruits are usually irregular, so using a soft gripper an autonomous machine can adapt to different sizes and shapes instantly due to its soft properties. The gripping force can be easily adjusted by its programming [7].

The goal of this project is to design and fabricate a pneumatically powered, functionally-graded soft robotic actuator made of a polymer embedded with nanoparticles, and later attach three of them into a hand-sized, remotely-controlled gripper assembly for object distribution.

3. Background

3.1. Literature Review

Significant research on soft robotics has been conducted over the past decade. Wearable robotic technologies for augmenting and restoring human performance are an important sub-field of rehabilitation engineering. Applications include biomedically enhancing or restoring

patient mobility (for limbs, fingers, or even organs) and manufacturing smart, minimally-invasive medical tools. An online collection of shared resources to support the design, fabrication, modeling, characterization, and control of soft robotic devices is available as the Soft Robotics Toolkit. These resources include CAD files, modeling instructions, and even guidelines for 3D printing molds for casting and fabrication of soft robotic polymers. It even provides links to the supplies required and case studies for modeling and characterizing these soft components.

Another important development is microfabrication for biologically-inspired robots. Current research involves new micro- and meso-scale manufacturing techniques, fluid mechanics of low Reynolds number flapping wings, control of sensor-limited and computation-limited systems, active soft materials, wearable robots, and morphable soft-bodied robots. Research teams have developed the first entirely soft autonomous robot, the Octobot, made by 3D printing, molding, and soft lithography. It is powered chemically and controlled by microfluidic logic. Another development includes soft robotic grippers for deep-sea exploration and handling delicate specimens. They can be designed and programmed to exhibit a complex range of motions.

Furthermore, a research team has also 3D-printed a functionally-graded soft robot powered by combustion. Multi-material 3D printing can generate a gradient from soft to hard materials in a monolithic body to reduce stress concentrations. The robot jumps through inflation of elastic bladders. The long-term vision with these soft robots is to bridge their coexistence with humans by making them inherently safer to interact with. They are optimal for compliance and adaptability in natural environments. Applying them to human limbs can enhance and augment the mobility of healthy individuals, as with the soft exosuit and soft robotic glove. The glove in particular can offer reinstated mobility to people with arthritis, locked trigger finger, or various injuries. The alternate rigid devices, while available and capable for many of the same tasks, possess excessive mass and kinematic restrictions.

Many other drastic developments in the field of soft robotics have been made worldwide.

Soft, pneumatic, flexible rubber microactuators with 7 degrees of freedom can twist, bend, walk, hold beakers, rotate them, and screw in a screw, the latter being demonstrated in Figure 3.1 [8].

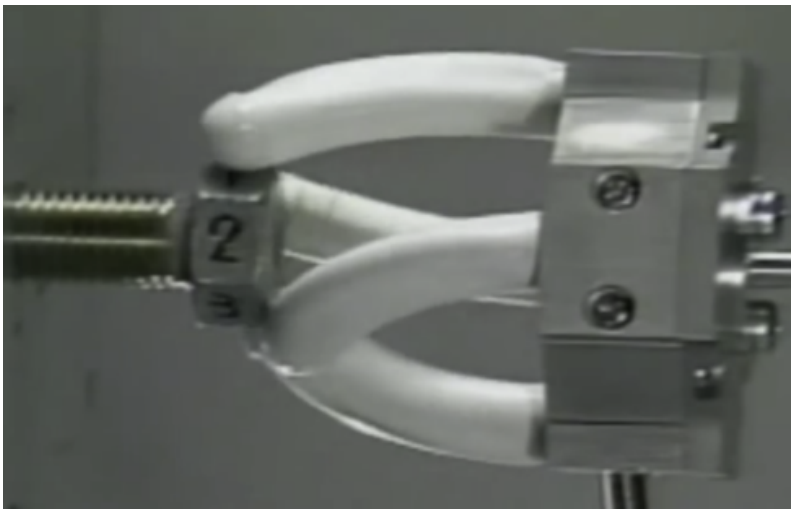

Figure 3.1.: A gripper of four 7-DoF pneumatic rubber microactuators screwing in a screw [8].

Its manipulation skills are extremely impressive, and many researchers have worked hard to create actuators with such dexterity. Their interests pushed them on to implement these McKibben actuators (pneumatic artificial muscles, or PAM's) to a thin musculoskeletal lower-limb robot driven by multifilament muscles [9]. Figure 3.2 shows them attached to a human skeleton model in standard leg motion positions.

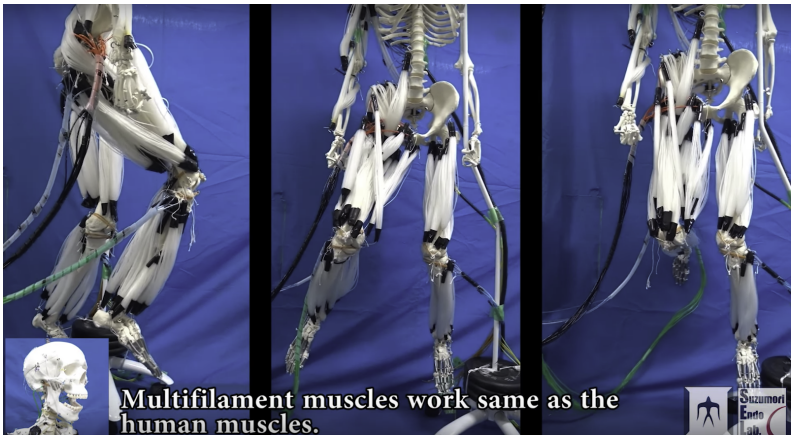

Figure 3.2.: Pneumatically-operated artificial muscles controlling skeletal limbs [9].

Other laboratories making developments in soft robotics apply biological principles in the design, fabrication, and control of new types of machines like soft robots. Some researchers have have presented a soft robot design that uses voice coil actuators integrated into a soft body to achieve worm-like peristaltic locomotion. Specifically, bio-inspired SoftWorm robots, based on the anatomy of the caterpillar, have been fabricated by vacuum casting silicone elastomers into 3D-printed molds, while currently being printed in a soft rubbery polymer using a multi-material 3D printer. The worms are actuated with shape-memory alloy (SMA) microcoils that can be controlled with current pulses [10]. With this design they are able to crawl, inch, roll, and even climb steep inclines. A projected application for the future is creating autonomous worms safe enough to swallow to help diagnose diseases or deliver medications [11].

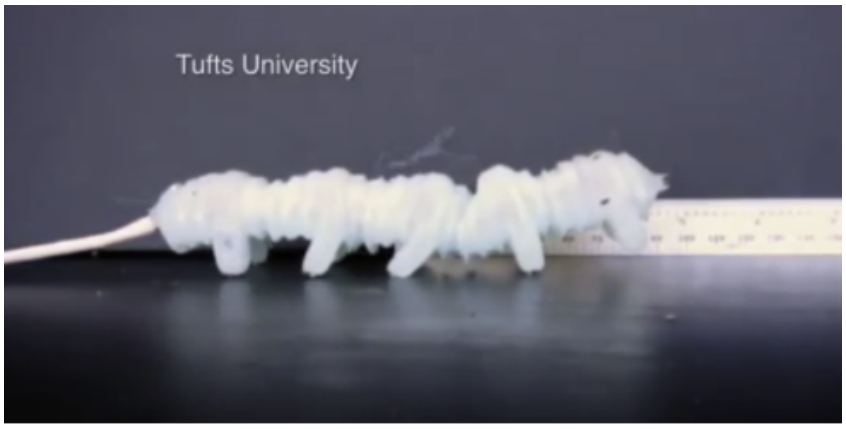

Figure 3.3.: Bio-inspired soft robotic caterpillar [12].

One more important project in soft robotic research is the design and development of a soft-bodied robot inspired by the octopus, an "ideal model for soft robotics and morphological computation." By investigating the fundamentals of octopus dexterity, this research led to a robot, based broadly on the anatomy of the octopus body, with locomotion and grasping capabilities [13]. The idea is to make use of similar octopus dexterity, speed, control, flexibility, and applicability in water. The octopus "represents a paradigm of the tight relation between morphology and behavior, and an 'animal model' for soft robotics technologies" [14]. Furthermore, its true continuum actuator challenges the primacy of joint space

and the notion that a finite number of relative displacements between individual links must describe robot behavior [6]. With these types of actuators the team sees many applications, especially in the biomedical industry, for soft arms that can navigate natural and complex yet minimally invasive surgical environments with high precision and control.

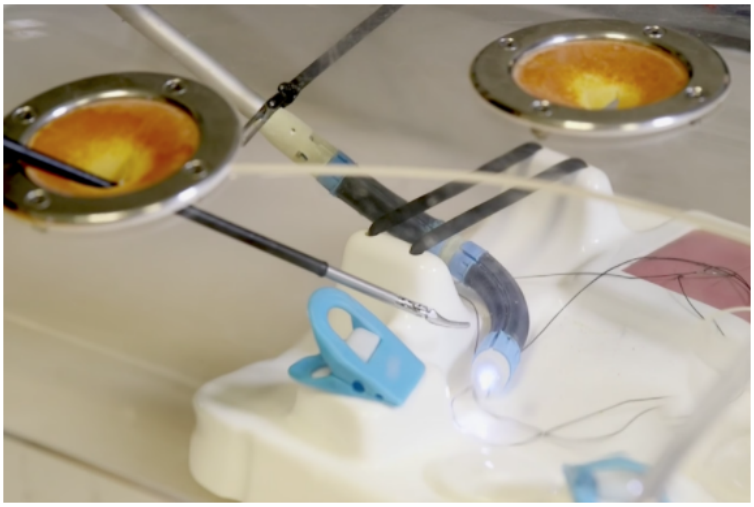

Figure 3.4.: Soft actuator for minimally invasive surgery [15].

3.2. Materials Modeling

The finite element analysis (FEA) program Abaqus was used in this project to model and analyze the actuator, and was also used to create visualizations of the output results of the simulations. For manufacturing, the 3D modeling program SolidWorks was used to design the actuator's mold, funnel, and the gripper's triple-actuator fixture. With the virtual model, the prototype can be visualized and the design can be adjusted before production of a physical version.

Every analysis by Abaqus consists of three main stages: Pre-processing, Evaluation, and Post-processing. Pre-processing is the where to all parameters are defined by the user for the analysis. First, a user can use the "Create Parts" feature to create the model parts. Abaqus provides a sufficient amount of tools to create a model with basic geometry features. Alternatively, the user can create a model by using computer-aided design (CAD) software

and then import it to Abaqus. All geometric dimensions at this point should be defined. After the model is built, especially in this project's case, a partition line has to be drawn on the model, in order to apply different materials to different sections in later steps. Next, material properties should be input and stored. This project's material is elastic, and basic properties such as Young's modulus and poisson ratio are entered. Two materials had to be defined in this project. Then, the "Section Module" allows users to assign different material to parts. In this case, sections had to be created and two sections assigned that are separated by the partition line. Assembling is done right after the previous step. Given that there is only one part in this simulation the assembly stage was skipped. "Step Modulus" allows the user to assign different variables in different steps, such as changing loading gradually throughout time. The internal pressure inside the actuator is the only applied force in this case. It is useful to determine the corresponding curvature of the actuator according to the applied pressure. After the loads are created on the model, boundary conditions need to be set, and in this case it would be the open end face with all degrees of freedom constrained ("Encastre"). Then, meshing is required for finite element analysis. The more nodes that are created in the analysis, the more accurate are the results that Abaqus is able to produce. At this point, the pre-processing part is done, and can be submitted to initiate the evaluation by Abaqus. Once the result is done, in the post-processing step, the deformed shapes can be visualized step by step, and one can save the result data for future analysis, such as nodal displacement and element normal stress along its cross-sectional area.

3.3. Polymer Material Background

In order to properly implement a soft robotic system, a form of polymer manipulation may be considered. Most soft robotics systems use a liquid silicone rubber (LSR) as opposed to solid silicone rubber. LSR contains polymers with a lower molecular weight and shorter chains, making it a versatile material when combined with other components. There

are many components used to control the physical properties of plastic polymers, including crosslinkers, fillers, additives, stabilizers, and colorants. The curing process might also affect the end product. A crosslinker is used to turn the liquid rubber into a mechanically stable material. These commonly include peroxides or platinum catalyst systems. Once the crosslinker is added the to the LSR, the polymer will undergo a curing process during which it turns into a solid.

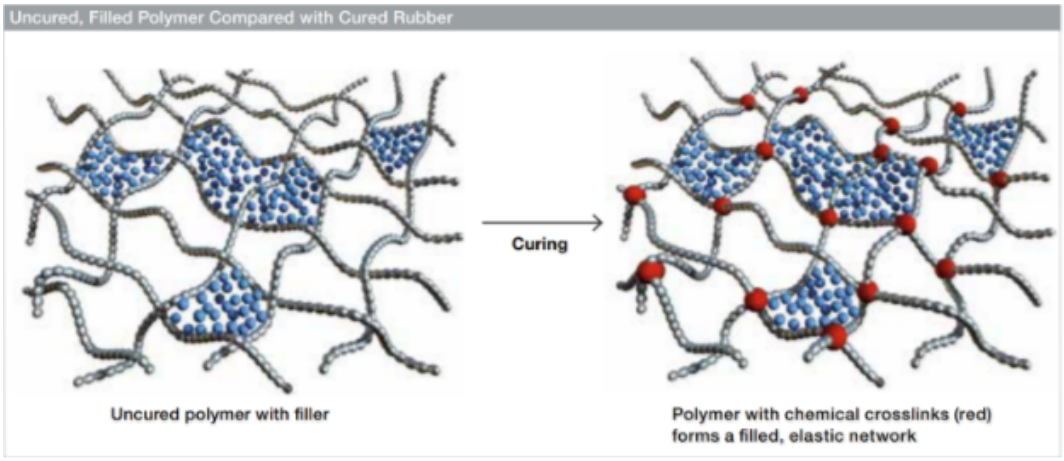

Figure 3.5.: Cured Polymer w/ cross-linkers [15].

A form of fillers is also useful to reinforce the silicone network. The type of filler used has a large influence on the properties of the final rubber. Pyrogenic silica is the most common reinforcing filler used, as it helps reduce cost and improve the mechanical stability of the rubber in order for it to achieve the desired properties, such as tensile strength, elongation, break and tear strength. The fillers are usually prepared before being added to the LSR. Non-reinforcing fillers can also be added to reduce the tensile strength if that effect is desired.

Unlike other rubbers LSR requires very few additives. A stable compound can be achieved with only crosslinkers and fillers. Many types of rubbers might require accelerators or retarders, organic plasticizers, and organic antioxidants, in order to properly cure into a stable product. Other additives that might be also added to SLR might include stabilizers, masticating aids, and colorants, but they are not required.

Stabilizers may be used for special applications in order to improve properties like heat

resistance and resistance to other chemicals. These stabilizers typically include special oxides of transition metals (iron) and carbon. This project made use of iron oxide nanoparticles as a filler.

4. Materials and Methods

4.1. Methodology

The goal of this project was to design and fabricate a pneumatically powered, soft robotic actuator made of a polymer embedded with nanoparticles. In addition, casting three other layered actuators with functionally-graded properties ensures that the end of the actuator will have maximum flexibility and deflection while the part closer to the fixture will be stiffer and more stable. This section outlines the methods this team used to work towards the project goal. The team was split into two halves–a design team and a manufacturing team–to equally manage the tasks required for analysis and fabrication. A flowchart of the methods used is shown below:

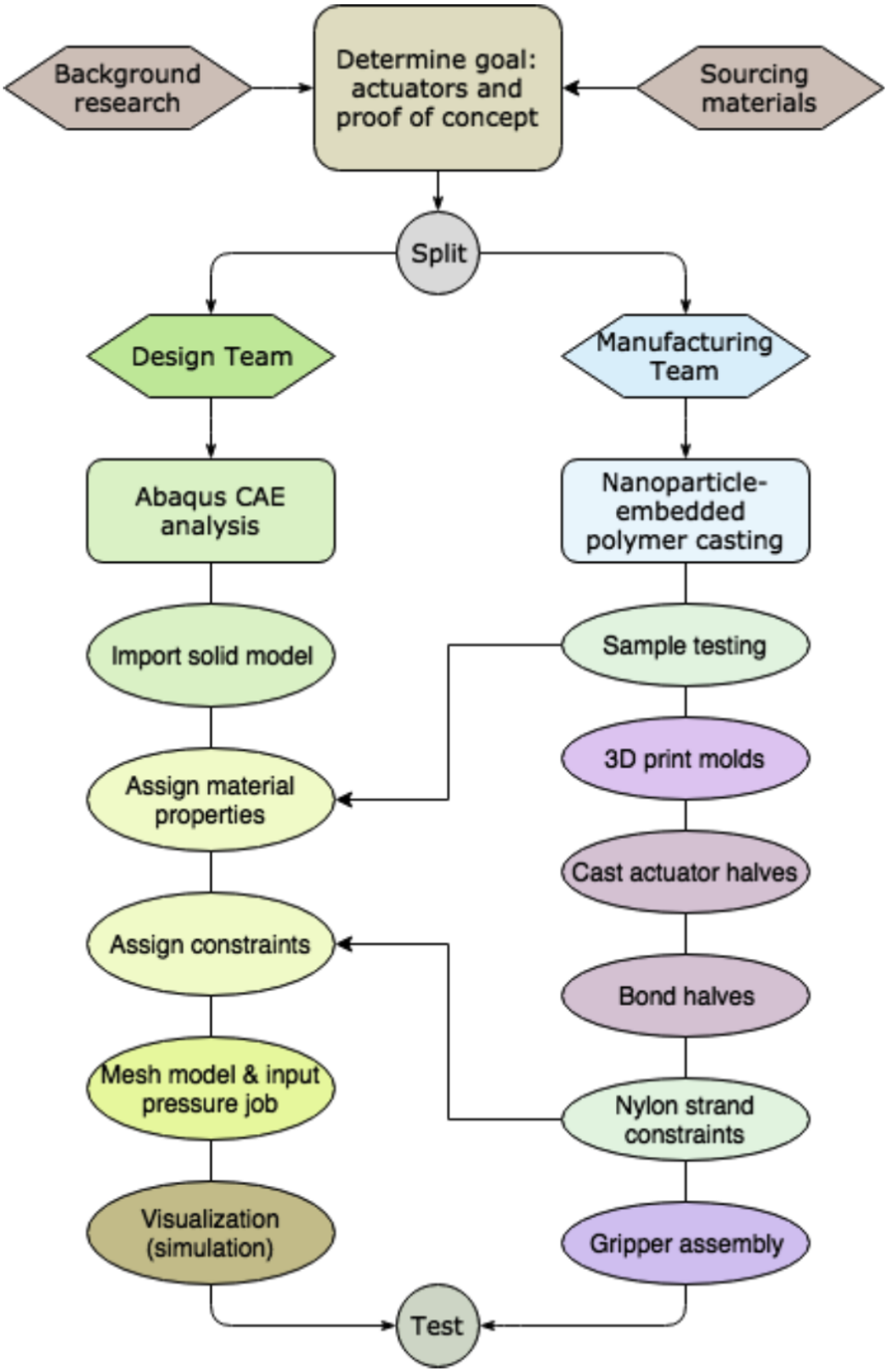

Figure 4.1.: Methods Flowchart.

4.2. Finite Element Analysis

Adequate analysis of a functionally-graded cylinder was required in order to determine the deformation and displacement given the dimensions and nanoparticle density of the actuator. The software of choice was Abaqus CAE for finite element analysis. The design team began by modeling the cylinder in Solidworks CAD for the main body of the actuator. All of the initial model dimensions were based off of the experiment in the Modeling, Integration, and Control of rPAMs methodology [18], and enlarged twofold according to the manufacturability with available machining equipment. The ID of the cylinder was set to 15mm and the OD to 20mm. Its length was set to 10cm. Previous work at the WPI civil engineering labs proved that Smooth-On Ecoflex and DragonSkin series silicone are both compatible polymers for the project goals. Material properties for Ecoflex, both with and without nanoparticles, were logged into the Materials module of Abaqus to be applied in their respective halves of the cylinder. Although the Ogden modulus is more accurate analyzing a hyperelastic material, the curve in the range of stress that the actuator would encounter during use was close enough to be considered linear. Therefore, Young's moduli from previous research [26] were input initially, and later the team's own testing results were used for the Abaqus model material properties [16].

Next, two different analyses were generated: the first one with the 15wt% elastic modulus on the nanoparticle half, and the other with the 4 divided sections assigned with different moduli (according to the tested stiffnesses of the dogbone sample testing) on the nanoparticle half. In the Steps module, the increments were defined as the levels of pneumatic pressure to be applied within the actuator; specifically 0, 0.5, 1, 1.5, 2, 2.5, and 3 psi (for iteration testing purposes). These were applied on the interior of the cylindrical model by selecting the proper surfaces and assigning them as sets. In the Load module the pressures were input as mechanical pressure. In order to model a constraint system against deformation by inflation (in the lateral direction), a series of 8 evenly-spaced 1-mm wide rings were added to the model and assigned the mechanical properties of nylon, as that was the flexible adhesive

material to be used for the actuator constraint.

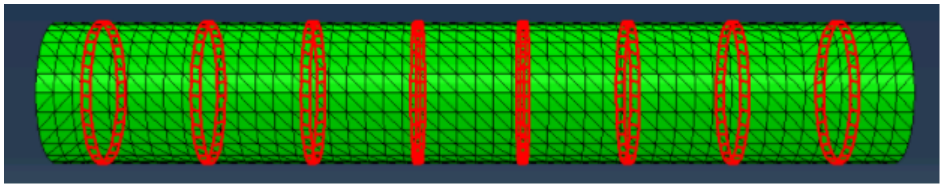

Figure 4.2.: Assembly for Actuator and Ring.

The boundary conditions were assigned at the uncapped face of the cylinder, with the Encastre feature used as the BC of choice to fix that face according to all the axes. All degrees of freedom at that face were constrained. Next, a mesh of the solid model was created for the actuator model using the "tet" feature and quad-dominated for rings. The approximate size of the global seeds was set to 0.02 for higher resolution nodes.

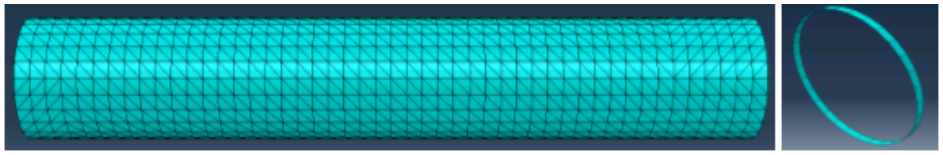

Figure 4.3.: Mesh for Actuator and Ring.

Finally, a Job was created at standard settings and subsequently submitted. It was Managed to check for errors before moving onto the Results tab to check the output database. Once the ODB was opened, the part deformation could be viewed in the Visualizer. The deformation scale factor was maintained at 1.

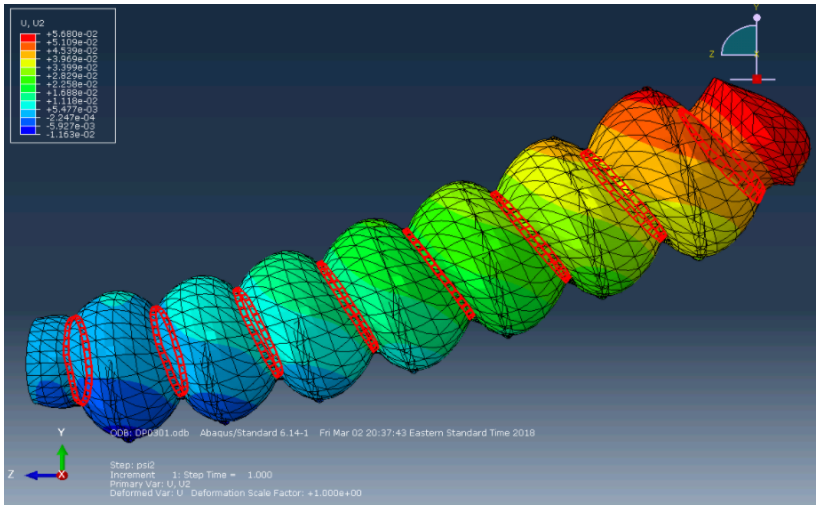

Figure 4.4.: Actuator deformation in the 2psi step of the Abaqus simulation.

At this point the model could be tested for deformation and pressure statistics. For analyzing the force that can be generated from an actuator, an extra boundary condition was defined at the end section of the actuator. The fixture was assigned to reflect the contact area that the actuator would make when contacting a certain object, as in a mechanical gripper. Therefore, the fixture face was assigned at the top of the end of the cylinder exterior with the Encastre feature.

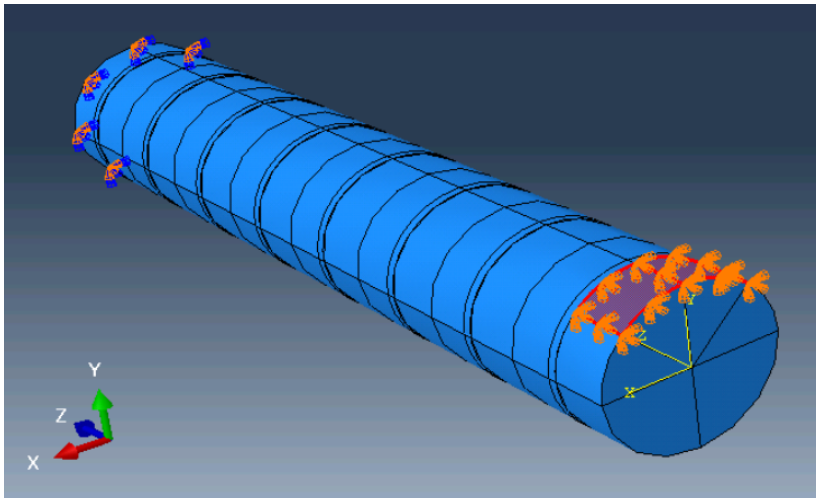

Figure 4.5.: Boundary Conditions for Analyzing the Reaction Force.

After the calculations from Abaqus, the OBD field output feature was selected. As shown in Figure 4.6, the point of interest was selected as all nodes on the contact surface

(same as the fixture face as described above). Next, the results of the vertical forces on each of the nodes were summed to produce the total reaction force.

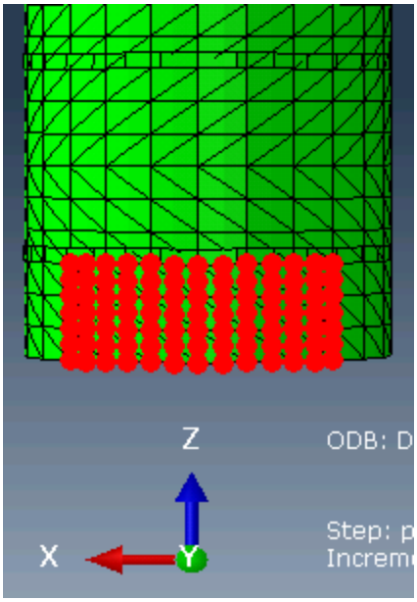

Figure 4.6.: Selected Nodes to Sum as Total Reaction Force.

4.3. Manufacturing Methods

In order to create the working actuator and demonstrate proof of concept for the functionally graded material, a manufacturing process and project plan were developed. The initial idea was to develop a method to produce consistent rubber polymers specified by the design. An LSR polymer (Ecoflex 0030) was mixed with a specific ratio of nanoparticles (0, 5, 10, 15 percent by mass) until the desired mechanical properties were met. This was achieved via a process of testing and experimentation using a variety of material testing equipment in labs available to the team. Once the method of casting polymers was established, the team then proceeded to making molds on a Flash-Forge Creator Pro 3D printer, based on the dimensions of the computer simulated design. These molds were sprayed with a primer to ensure non-permeability. This allowed the team to deposit pure polymer, mixed proportions, and layered combinations in order to achieve both the half-and-half (15wt%

nanoparticle half) and the functionally graded (0, 5, 10, 15wt% layered) actuator halves. Both processes attempted to match the computer simulated models as close as possible.

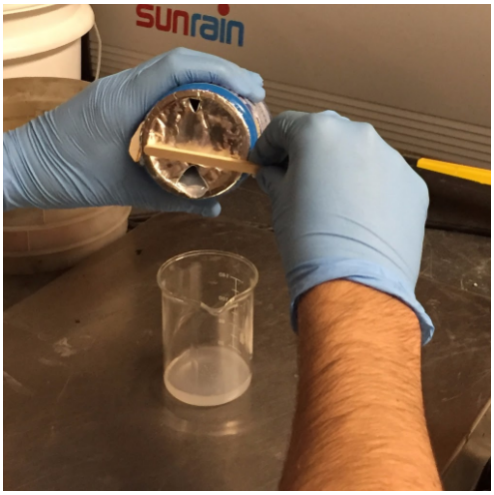

Figure 4.7.: Pouring Mixing Process.

Prior to the prototype construction and experimentation, materials were acquired. The team chose to go with Ecoflex 0030 according to its adequate material properties. For the nanoparticles, the team did some initial research to determine what type, size, and source to choose. Being less expensive, glass fibers seemed like a potential choice for a filler, so the team experimented with a 5% wt polymer mix using those. A large dogbone mold was 3D printed and sprayed with Rustoleum 2-in-one primer to avoid having the silicone fuse or settle into the permeable print. This would also help removal once the silicone cured. In that mold, a dogbone sample was cast and cured in under 24 hours. Tensile testing was done on the sample using an Instron machine. After getting undesirable results (what appeared to be plastic deformation), the glass fibers were abandoned and the team looked at more potential nanoparticles, even considering microparticles for their less expensive cost. Fortunately, graduate student Kwabena Kan-Dapaah had done similar research and suggested using the same iron-oxide compound that he used for his project. In that experiment, he used proportions of 0, 5, and 10 wt% [19]. Its size and price seemed adequate for this project's standards, so the "Magnetite," as it is called, was ordered. Specifically, the team ordered

"Iron Oxide Nanopowder / Nanoparticles (Fe2O3, gamma, high purity, 99.5+%, 20 nm)." [20]

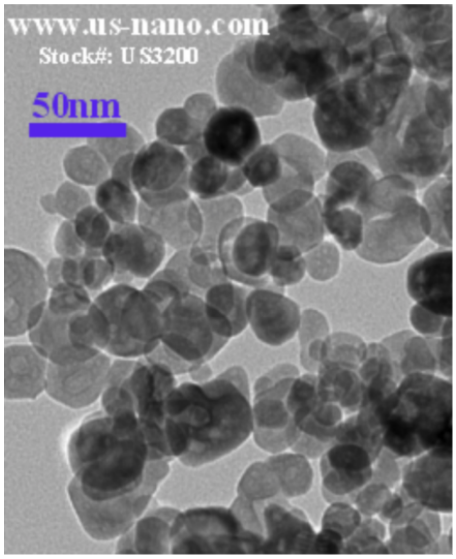

Figure 4.8.: Transmission electron microscopy (TEM) image of the magnetite powder [3].

The team also borrowed a six-dogbone metal mold from that same graduate student to begin casting and testing the material mix. To cast the Ecoflex 0030 silicone, the procedure included combining the two components of the binary mixture in an even 1A:1B ratio, in a beaker on a scale. A popsicle stick was used to carefully get the accurate amount of liquid silicone into the beaker, typically about 10g of each LSR component. Once in the beaker, the components were mixed and swirled together to get a uniform blend. With the silicone solution infused with air bubbles, a method was needed to deaerate the solution, which was initially done using a shake-table in the laboratory. This method worked for a pure silicone casting, but proved to be problematic with silicone-magnetite mixes when the team noted that it increased the rate that the nanoparticles would settle out to the bottom of the solution prior to and during casting.

Initially, a pure silicone control sample was cast for tensile testing. The team allowed for the air bubbles to leave the wet mix by placing the mold and sample on a mixing table for 25 minutes, ensuring that the setup was level (using a level). After curing, it

was tested via Instron tensile machine. For the mixtures, several different dogbone samples were cast, using about 10g of Ecoflex combined with 4%, 8%, 12%, and 16% magnetite weight fractions. Previous research and laboratory testing has proven that 20% is excessive and causes magnetite settling in the solution. To avoid the settling issue with the heavier combinations, immediately after mixing, the beaker was placed into a vacuum chamber at 25 mmHg to remove the air bubbles. This could typically be achieved in about 5 minutes.

Figure 4.9.: Vacuum Chamber Gauge.

After air bubble removal, the mixes were poured into respective dogbone molds and allowed to cure. A series of dogbone profiles were cut out of an 1/8" thick sheet of acrylic for this purpose. Each of the five wt% mixes had three cutouts for reliable data from the testing. The chosen dimensions for the dogbone samples, according to the compatibility with the 50N tensile microtester, are as follows:

Dimensions	W	T	L
Inch	0.1	0.115	0.55

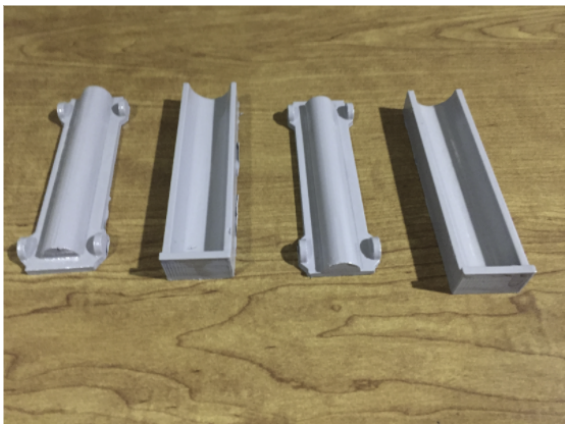

Figure 4.10.: Primed, 3D-printed actuator half molds

The team then machined a cylinder out of aluminum with an OD equal to the actuator's ID. This was used as a mandrel for gluing the two halves of the cast actuator together. The molds for the actuators halves were each 3D printed according to the desired dimensions for half of the actuator. Upon one cast, it was noted that the liquid silicone would spill over easily when being poured into the mold. Therefore, the team 3D printed a funnel for pouring the polymer mix into the mold more efficiently. It was fitted onto the top of the mold before pouring.

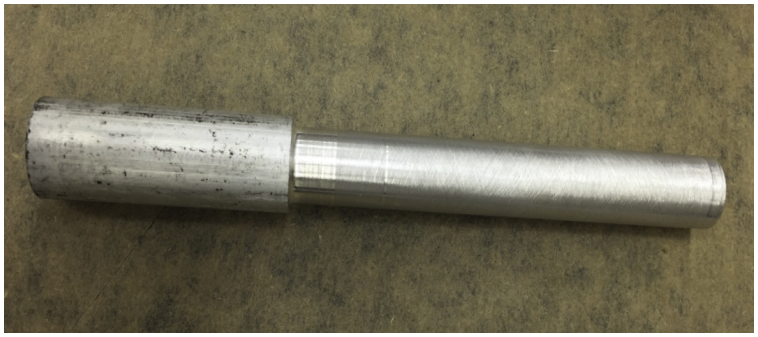

Figure 4.11.: Aluminum Mandrel for Actuator Half-Bonding.

For the clear half of the actuator, the pure Ecoflex was poured into one of the molds and allowed to cure. For the stiffer part of the half-and-half actuator, a 15% magnetite mix was poured into the mold and allowed to cure. For the layered actuators, to demonstrate functionally-graded properties, a special mold was made, with a 0.125"-thick clear acrylic

backing to be able to see the polymer being poured into the mold during the process. Furthermore, a silicone pigment was purchased to mix with the uncured Ecoflex before pouring those portions of the functionally-graded (FGM) actuator, and distinguish one layer from another [21].

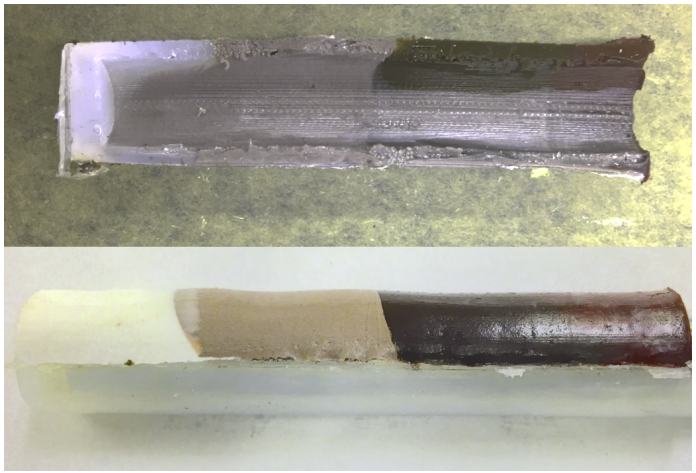

Figure 4.12.: The Functionally-Graded (layered) Actuators, making use of Silc Pig® dye.

During casting, a calculated amount of each of the 4 silicone mixes was poured into the mold sequentially, allowing just enough time to pass between pours so that the polymer had not solidified completely (20 minutes) to ensure proper bonding. This created the desired gradient in stiffness. The layers layers were consecutively poured into the mold, beginning with 0%, proceeding to 5%, then 10%, and finally topping it off with 15%. The ratios between layers were determined both lengthwise and volumetrically. The mold was marked by dividing the length of it into four equally-sized sections. To ensure proper volume and mass for each layer, the following calculations were done:

Cylinder OD: 2cm

Cylinder ID: 1.5cm

Full volume FV: $\pi * (OD/2)^2 * h = \pi * (2.0cm/2)^2 * 10cm = 31.4159cm^3$

Cavity volume CV: $\pi * (ID/2)^2 * h = \pi * (1.5cm/2)^2 * 9.5cm = 16.7879cm^3$

Actuator volume AV: $FV - CV = 31.4159 - 16.7879 = 14.6280cm^3$

Half of Actuator Volume HAV: $14.62802 = 7.3140cm^3$

One quarter of the HAV: $7.31404 = 1.8285cm^3$

Mass of Ecoflex (density=1.07) to be used: $1.8285cm^3 * (1.07g/cm^3) = 1.9565g$

Figure 4.13.: Silicone Adhesive for Bonding the Actuator Halves.

Permatex 80050 Clear RTV Silicone adhesive was purchased for mending the two halves of the actuator together. Since the silicone adhesive was advertised as a sealant, the team thought it might not bond the silicone, and purchased a secondary product known as Permabond, along with its corresponding primer. Upon testing on two disks of spare silicone, a plain one and a mixed one, this product proved to be ineffective since it dried too hard and inflexible. The original silicone adhesive was initially tested on more spare silicone and after three days it demonstrated very effective adhesion. It established a strong bond between the two samples and maintained full flexibility as well. This process was implemented on three pairs of actuator halves, for both the half-and-half and the FGM actuators. The pure Ecoflex half of the actuator was laid down along the inside of the 3D-printed mold used to cure it (sprayed with non-stick cooking spray to use as a removal lubricant or mold release), and the aluminum mandrel (also coated in the cooking spray) was then laid snugly within the actuator half. The silicone adhesive was evenly applied along the edge to be bonded. Next, the stiffer half of the actuator was pressed down on the mandrel, lined up properly with its corresponding half. The other half of the 3D-printed mold was then placed upon the assembly, and two mini C-clamps were applied to keep it pressed together firmly enough to bond.

Figure 4.14.: The Setup for Bonding the Two Halves of the Actuator.

After the two halves were bonded together, a constraining method was needed to stop the actuator from overinflating. The mechanical constraints were required to minimize outward expansion while not affecting elongation, since elongation allows the actuator to deflect or bend the desired amount when pneumatically pressurized. The idea was that as the actuator expanded, the constraints would keep it from inflating but permit elongation and deflection. This was accomplished by simply wrapping a series of adhesive nylon strips around the actuator. Initially, three rings were tested on an actuator and air was applied (Figure 4.15), but the material still expanded too much. Accordingly, the team next tried 10 rings spaced evenly along the 10cm length of the actuator (Figure 4.16), to ensure more coverage and prevent overinflation. This setup worked much better, with the constraints decreasing the amount of inflation while still allowing the actuator to properly extend and deflect.

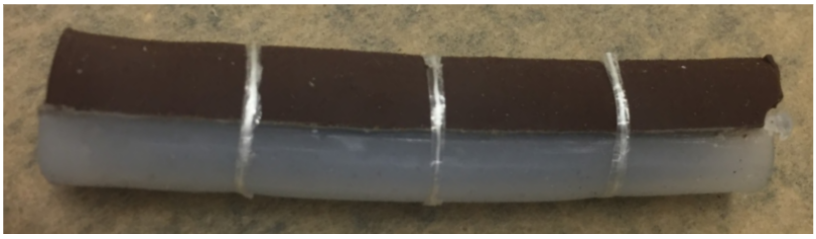

Figure 4.15.: The Three-Ringed Constraint Design.

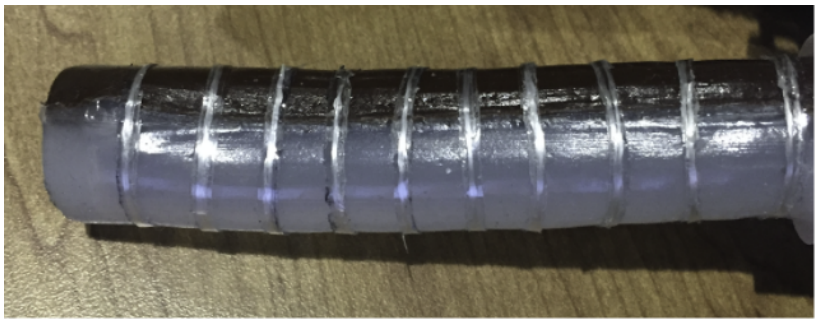

Figure 4.16.: The Ten-Ringed Constraint Design.

4.4. Method for Testing Stiffness

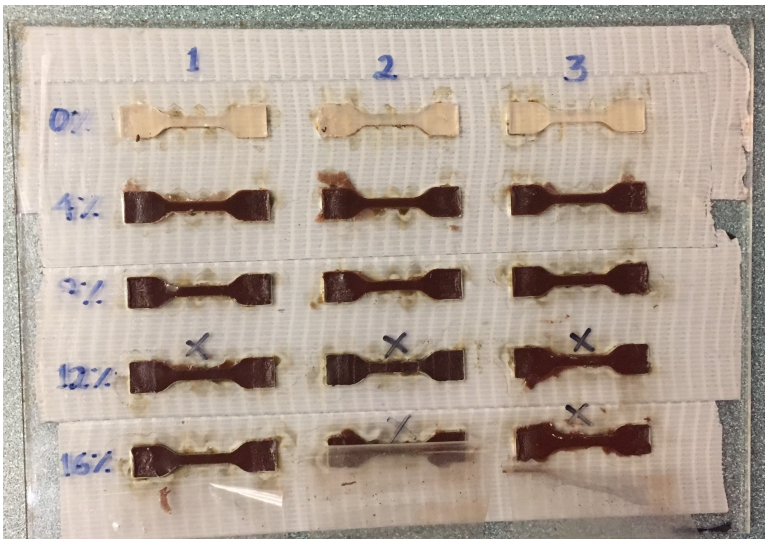

Figure 4.17.: Dogbone Acrylic Mold with Samples.

For mechanical property testing, the cured dogbone samples were removed, labeled, and placed into a 50N Instron testing machine to determine their stress-strain curves and eventually acquire a modulus of elasticity. To do this, the samples were secured into the grips. Next, the 5800 Console program was opened. The user must select the Balance Load button and reset the gauge length. Then one must start the test and monitor the progression on the load-extension graph. Next the data is saved at the end of the full extension (80 mm, or 5.7 strain) as a .raw file. Then the operator transfers the raw data to an Excel spreadsheet and plots it to acquire an approximate linear correlation with a slope that can be used as

the Young's Modulus for each polymer fraction mix. The Young's Moduli from the testing for the material properties were used on the mixed half of the FEA actuator model.

Figure 4.18.: One of the mixed dogbone samples under tensile testing on the Instron.

4.5. Control Systems

A control system was developed for the system, which is comprised of an Arduino microcontroller, the electronic pressure regulator, and a mechatronic arm. The full control system outlined in Figure 4.19 contains 3 sub-systems: a wearable gesture controller that receives input from the user's hand motions, a pneumatic system (using tubing, air regulation, and an air tank), and a mechatronic arm system that executes orders received wirelessly from the gesture controller. In Figure 4.19, the hard lines represent wire connections and the dashed lines represent wireless connections between components.

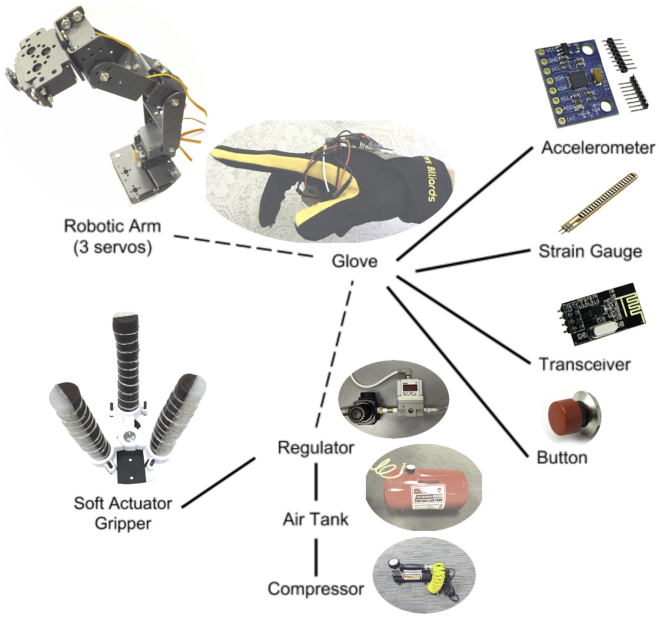

Figure 4.19.: Full system controls design diagram.

An Arduino Uno was used to control the actuators because of the ease of use and familiarity involved. In order to control the pressure within the actuators, a 0 - 5V DC signal must be sent to the electronic pressure regulator so that the setpoint pressure can be determined. The pressure range is set on the electronic regulator and the minimum and maximum pressures selected correspond with 0 and 5V DC, respectively. Then, using a Pulse Width Modulation (PWM) signal output generated by the Arduino as variable pseudo-analog signal, the pressure setpoint could be controlled electronically on the regulator.

4.6. Wireless Wearable Controller

The system is driven by a wireless wearable gesture controller. This is mounted to a glove that allows the user to control the pressure in the actuators by hand gesture. It is a patent-pending product that was designed and built by Jiacheng Liu using an Arduino, a single-board microcontroller. A strain gauge was placed under the middle figure of the glove to recognize the degree of bending, for the Arduino to translate the voltage feedback from the strain gage to pulse-width modulation (PWM) correspondingly. The PWM value

is transmitted through a 2.4GHz RF transceiver on the glove to another transceiver that is linked with another Arduino board to control the pressure output from a digital pneumatic regulator. The controller also includes an accelerometer on the controller, which is used to control the positions of the gripper's robotic arm, also with PWM. Hand roll generates robot arm yaw (revolution about the base), and hand pitch generates robot arm extension and contraction (reaching out or pulling back).

Figure 4.20.: The wireless wearable gesture controller.

4.7. Pneumatic System

An ITV101121NBL4 electronic pressure regulator was purchased according to the specifications required for Arduino control and 0-5 psi output. The specifications of the particular electronic pressure regulator were as follows: 0.001MPa to 0.1MPa output pressure range (0.145 - 14.5psi), 12 - 15V DC supply range, and 0 - 5V DC input signal range. The output pressure range could be set and mapped to an analog input signal ranging from 0 - 5V DC.

A fastener for the head of the actuator was used to transfer air pressure from an 11-gallon Torin Big Red portable horizontal air tank. In the first stage out of the tank, a manual pressure regulator, made by ARO-Ingersoll Rand, was connected to regulate the tank's air pressure to an optimal pressure for the SMC electronic pressure regulator. The second stage of pressure regulation involved the SMC electronic pressure regulator, which was used for quick and precise control over the air pressure being delivered to the actuators. It allows for both increasing and decreasing the input pressure.

Figure 4.21.: The air tank, power source, and pressure regulators.

The fixtures at the entryway to the actuator were designed on modeling software and then 3D printed. The engineering drawing for their design is presented in Appendix C. There was concern over the possibility of air leaking out from the material not being airtight enough, and initial testing proved this to be the case, as air could be heard escaping. Teflon tape was used to seal it, along with a 3D-printed insert with higher infill. Furthermore, the potential deflection could not be maximized given the geometry of the three-way fixture. In order to allow proper deflection of the actuators and sufficient pressure applied upon the object of choice, the fixtures were set at an obtuse angle to have the actuators far enough apart from each other.

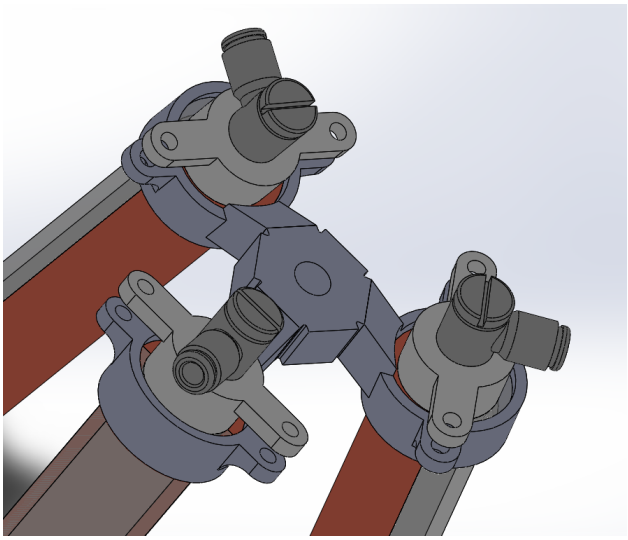

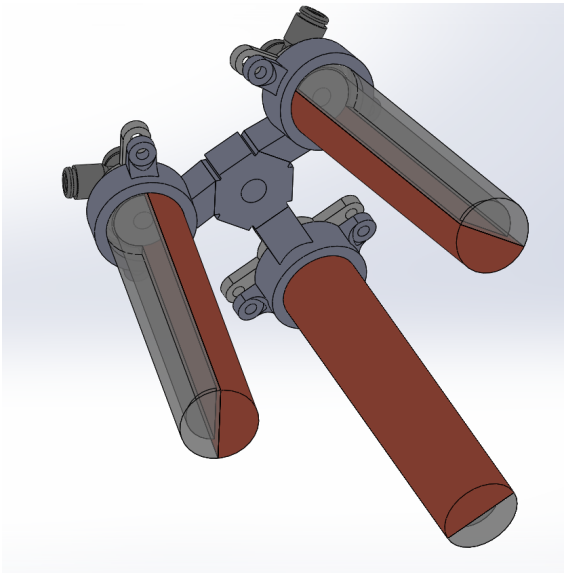

Figure 4.22.: Gripper CAD Model.

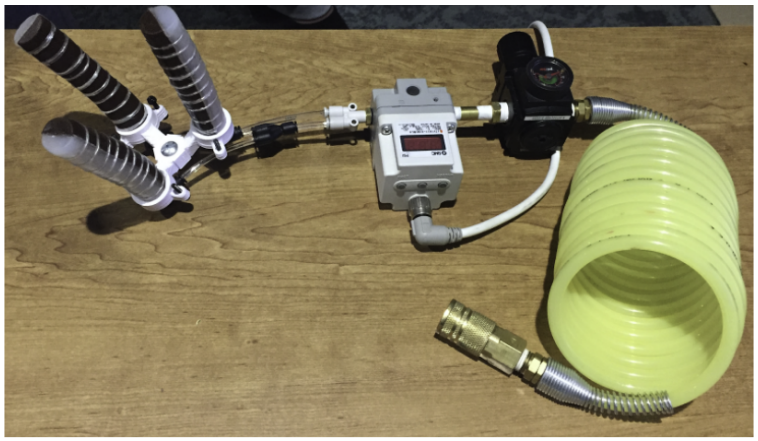

Figure 4.23.: Pneumatic Control System Equipment.

4.8. Mechatronic Robotic Arm System

The mechatronic arm system was built with a three-degree-of-freedom (3-DoF) robotic arm in an RRR (revolute-revolute-revolute) configuration (Figure 4.24). It was built with three standard-sized hobby servos. The platform of the gripper was configured to be always parallel to the ground. The two servos on the wrist and elbow joints are controlled by the pitch angle of the wearable gesture controller. The third servo, on the base of the robot, is controlled by the roll angle of the wearable gesture controller. These features compose a robotic assembly which allows for the gripper to be manipulated in 3-dimensional space. The specific movements that were achieved consisted of reaching down, gripping an object, and then picking it up and transporting it to an assigned location. The robotic arm is connected to the same Arduino microcontroller that controls the pneumatic system.

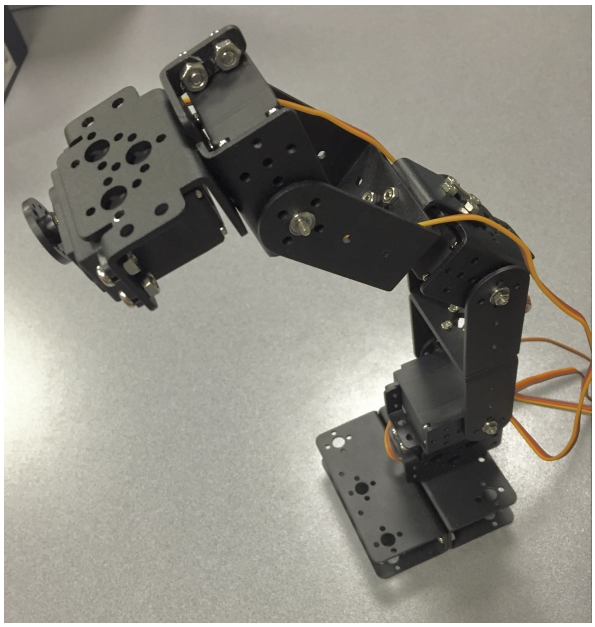

Figure 4.24.: The Robotic Arm as a Part of the Mechatronic System.

The workspace of the robot arm can be described as a half-semispherical space. Constraining the rotation of the arm to half of a full rotation prevented the wires and pneumatic tubing from tangling or binding. Initially, the robot arm was built with a greater number of degrees of freedom. It was then simplified to better conform to reasonable weight and power limitations while still being able to meet the needs of manipulating the gripper.

4.9. Testing Method for Force Output and Deformation

The actuator was tested through both the design and the manufacturing process. For design, the actuator was tested on the Abaqus program to determine displacement and pressure values. On the physical side, the gripper was placed on a scale that could measure the applied pressure at different inputs (0, 0.5, 1, 1.5, and 2 psi).

The force that an actuator can apply laterally was tested using an electronic scale as shown in Figure 4.26. The measurement was done by placing the actuator on the scale and making sure the contact area was at the side of the front end as it was simulated by Abaqus as shown previously. First, the scale was zeroed when the actuator was at the atmospheric

pressure under the weight of the actuator. Then, the pressure was increased by steps of 0.5 psi. Due to the limitation of the pressure regulator, the input pressure ranged from 0.5 psi to 2 psi. Therefore, the data of force was recorded with three trials at input pressures of 0, 1, 1.5, and 2 psi.

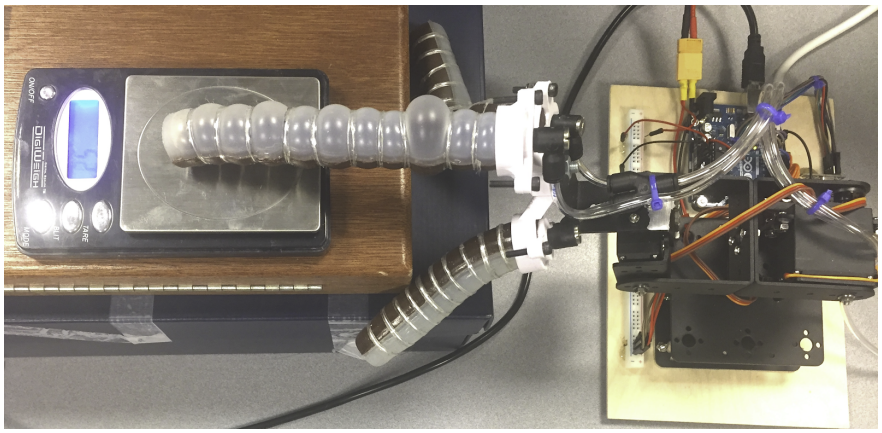

Figure 4.25.: Testing Method for Finding the Force Output.

The actuator's lateral deformation was tested using a ruler. Same settings for input pressures were used as in the tests for force. A standard ruler was used to approximate the result. The setup is shown in Figure 4.26.

Figure 4.26.: Testing Method for Finding the Lateral Deformation.

Once the entire gripper assembly was fully operational and controlled by the remote gesture glove, it was tested by picking up an egg shell, swinging it around, and placing it in a targeted disposal zone.

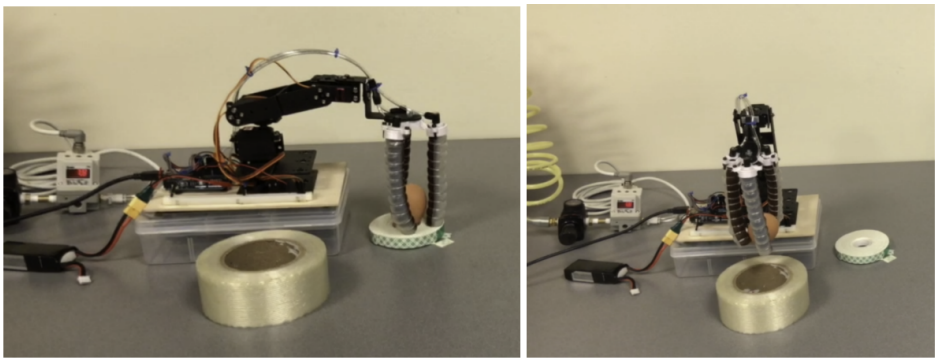

Figure 4.27.: Remote testing of the robotic gripper using an egg shell for object redistribution.

5. Results

The goal of this study is to understand the relationship between concentrations of nanoparticles in the polymer Ecoflex and its mechanical material properties, particularly its Young's Moduli. The varying stiffnesses designed and manufactured in the layered actuators allow for desired bending motion in the final actuator assembly. The effect of the gradient in stiffness is further explored through finite elements analysis, and its results are also presented here.

5.1. Polymer Sample Tensile Testing Results

The results in the figures show that as elongation increases and the stiffness properties of the samples are tested, the slopes of the curves generally follow a hyperelastic model. Given the repeated tests done to check the hypothesis that higher concentrations of nanoparticles demonstrate a higher Young's Modulus, the data proves this initial concept correct. The control in this experiment is the 0 wt% dogbone samples, which demonstrated the greatest elongation, as predicted. Initial batches of samples were larger in size. Months after casting them, the team noticed that the moisture content in the samples, which had been laid out on paper, had gradually drained out, to a degree. The samples did not seem as moist as the freshly cast ones and the paper appeared oily. Consequently, smaller dogbone samples were cast and the testing was done shortly after (within a week), to ensure properties remained the same. In the end, a laser-cut mold was used with each polymer-nanoparticle mixture

having three samples each to later average out the tensile testing results.

Three dogbone samples (standard microtester size) were used for testing each mix ratio, and their stress vs. strain curves are shown in Figure X, with their corresponding linear equations and correlation values. The slopes of the equations are all very close in magnitude at approximately 24,100. Stress is measured in Pascals.

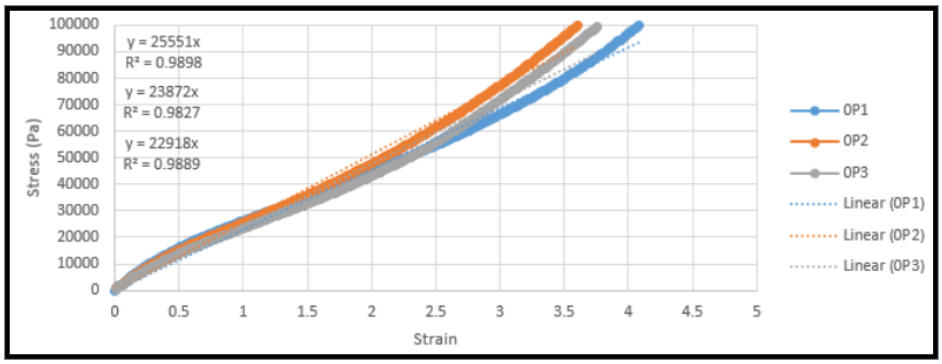

Figure 5.1.: Example of Stress Strain Curve with plain EcoFlex 00-30 specimen.

The summary of all the results (for 0, 4, 8, 12, and 16 %wt) indicates that as magnetite (Fe2O3) wt% increases, material stiffness also increases. A linear regression line was created from the experimental data which represents the relationship between percent weight of magnetite and the elastic modulus. As demonstrated in Table X, using the linear model, this relation enables approximation of the elastic modulus for any given percent weight of magnetite, which in our case was 0, 5, 10, and 15 percent for our functionally graded actuator (FGM) design. These calculated elastic moduli were used in the FEA model.

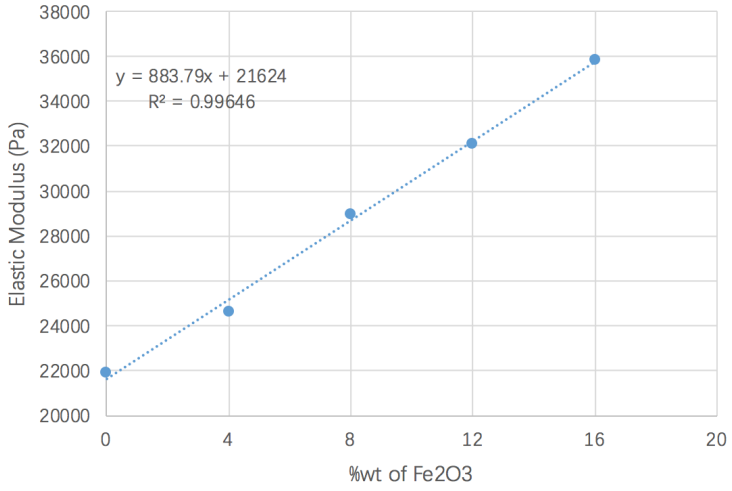

Figure 5.2.: Plot of %wt of Fe2O3 versus Elastic Modulus.

%wt of Fe2O3	Calculated Elastic Modulus (Pa)
0	23270
5	28172
10	33075
15	37977

Figure 5.3.: Calculated Elastic Modulus Corresponding to Percent Weight of Magnetite.

5.2. Finite Element Analysis Simulation Results

Using the experimental data, the appropriate material properties could be assigned in the Abaqus program for simulation and determination of force and displacement. The following graphs (and the respective linear equations and correlation values) were constructed from the results of the FEA simulations. Figure 5.2 shows that at 15 kPa of input pressure applied on the inner walls of the FGM actuator, its furthest end should displace about 60mm.

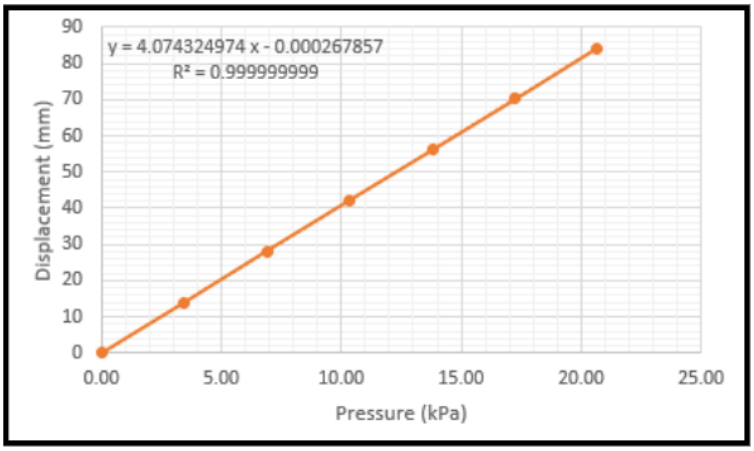

Figure 5.4.: Plot of Displacement versus Pressure for the FGM model.

Figure 5.5 shows that at 15 kPa of input pressure applied on the inner walls of the functionally-graded actuator, its furthest end should apply about 130mN of normal force onto whatever object the gripper may be grasping.

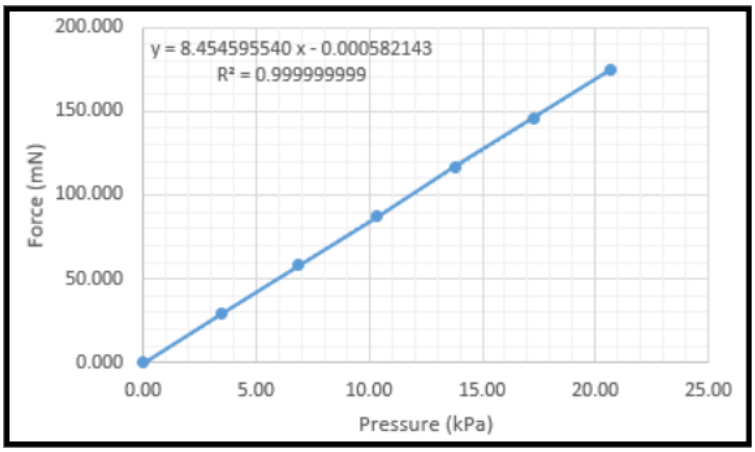

Figure 5.5.: Plot of Reaction Force versus Pressure for the FGM model.

These values are clarified in Figure 5.6, which specifies the FEA job output from the simulation at various input pressures. Given the standard range of soft robotic actuators of this size, the input pressure ranged from 0 to 3, with 0.5 psi increments. Force and displacement simulation results are presented below.

Pressure		Force		Displacement
Psi	kPa	mN	g-force	mm
0	0.00	0.000	0.000	0
0.5	3.45	29.143	2.972	14.0443
1	6.89	58.295	5.944	28.0927
1.5	10.34	87.438	8.916	42.137
2	13.79	116.581	11.888	56.1813
2.5	17.24	145.733	14.861	70.2296
3	20.68	174.876	17.832	84.2739

Figure 5.6.: Reaction Forces Resulted by Input Pressure for the FGM model.

Results were determined according to the same procedure for the half-and-half model (half pure silicone, half 15%wt magnetite). Figure 5.7 shows its displacement vs. pressure plot. Results show that at 15kPa the half-and-half actuator is to demonstrate just under 80mm of displacement, more than the FGM actuator.

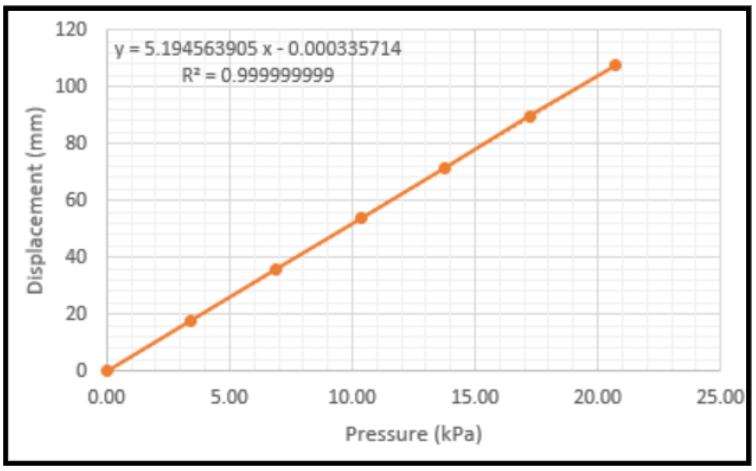

Figure 5.7.: Plot of Displacement versus Pressure for the Half & Half model.

Figure 5.8 shows the reaction force vs. pressure plot, with an expected output of about 120mN at 15kPa of input pressure.

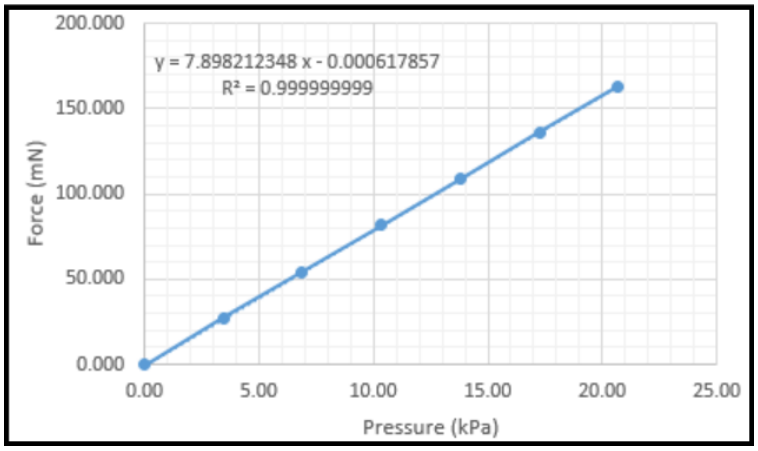

Figure 5.8.: Plot of Reaction Force versus Pressure for the Half & Half model.

Figure 5.9 shows the summary of these input parameters and simulated outputs. Given the standard range of soft robotic actuators of this size, the input pressure ranged from 0 to 3, with 0.5 psi increments. Force and displacement simulation results are presented below.

Pressure		Force		Displacement
Psi	kPa	mN	g-force	mm
0	0.00	0.000	0.000	0
0.5	3.45	27.225	2.776	17.9058
1	6.89	54.459	5.553	35.8168
1.5	10.34	81.684	8.329	53.7226
2	13.79	108.909	11.106	71.6284
2.5	17.24	136.142	13.883	89.5394
3	20.68	163.368	16.659	107.445

Figure 5.9.: Reaction Forces from Input Pressure for the Half & Half model.

5.3. Comparison of Analytical and Experimental Data

Aside from the FEA model simulation, the physical actuators were also tested after being mounted to the triple-headed gripper to see what pressure they could apply on a scale. For an initial test, at 2 psi of pressure input, the gripper was able to pick up a 12g cylindrical object. Once the mechatronic arm was fully operational and controlled by the remote gesture glove, it was tested by picking up an egg shell, swinging it around, and placing it in a targeted disposal zone. To determine what lateral forces the actuators applied onto

the object being gripped, the actuators were placed on a digital scale and zeroed at 0.5 psi to measure the applied force at stepped input pressures. To determine lateral deflection a ruler was placed perpendicular to the vertically-hanging actuator before it was pressurized. The half-and-half actuator was tested first, at 1, 1.5, and 2 psi of air pressure. Applying any more pressure seemed risky given the integrity of the actuator adhesion line, the ring constraints, and the seal at the fixture (which needed to remain airtight for actuation). Output forces and displacements are presented on Figure 5.10 in Imperial and SI units.

Pressure		Actual Force			Experimental Displacement		
Psi	kPa	g-force	mN	% Difference	in	mm	% Difference
0	0.00						
0.5	3.45						
1	6.89	5.933	58.186	6.845	0.3	6.4	82.271
1.5	10.34	6.467	63.416	22.364	0.7	16.5	69.268
2	13.79	8.933	87.606	19.560	1.4	36.4	49.173
2.5	17.24						
3	20.68						

Figure 5.10.: Measured Reaction Forces and Displacement for the Half & Half model.

The same tests were conducted for the functionally-graded actuators mounted on the gripper. Figure 5.11 shows the measured force and displacement values at 1, 1.5, and 2 psi of air pressure. Output values are presented in SI and Imperial units.

Pressure		Experimental Force			Experimental Displacement		
Psi	kPa	g-force	mN	% Difference	in	mm	% Difference
0	0.00						
0.5	3.45						
1	6.89	7.267	71.262	22.243	0.7	17.9	36.318
1.5	10.34	11.333	111.142	27.109	1.4	36.6	13.037
2	13.79	14.033	137.620	18.047	2.8	72.1	28.293
2.5	17.24						
3	20.68						

Figure 5.11.: Measured Reaction Forces and Displacement for the FGM model.

One of the observations noted during the testing stage was how the actuators tended to deflate slightly without any input air pressure. Their cross section approximated an oval more than a circle. For this reason, the system was set to apply a consistent 0.5 psi of

input air pressure even without the controller signaling for pressurization and extension of the gripper. The 1 to 3 psi range was deemed appropriate for gripper testing. Comparison graphs displaying the results from both the simulation and physical testing are shown below.

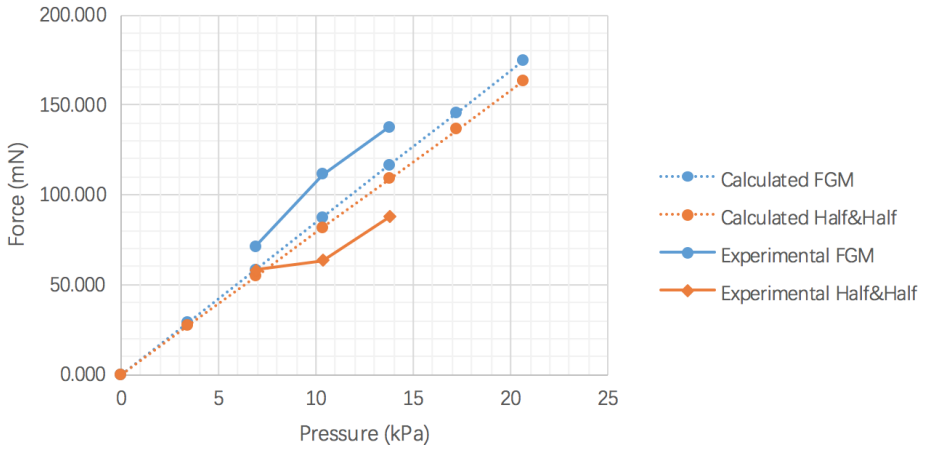

Figure 5.12.: Plot of Force vs. Pressure Results for Each of the Actuators.

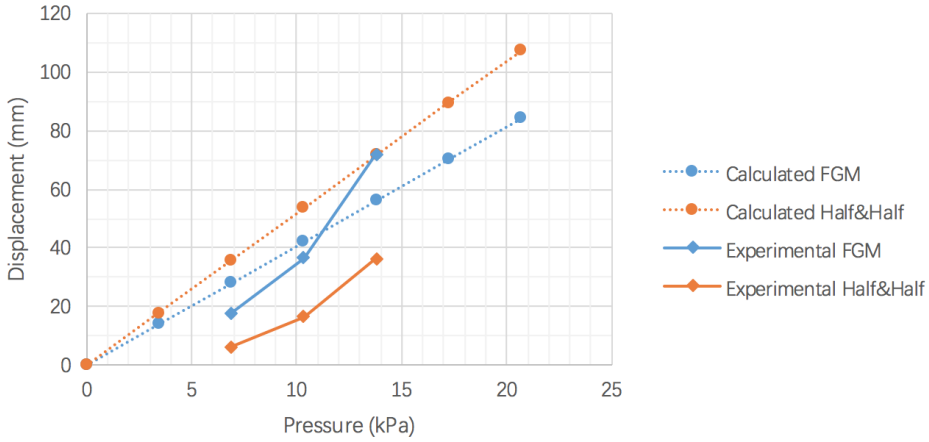

Figure 5.13.: Plot of Displacement versus Pressure Results for Each of the Actuators.

The graphs shown in figures 5.10 and 5.11 above demonstrate a summative comparison of the results from all the testing done through both the simulated actuator model and the physical project prototype. These results show that the relationship between input pressure and output force predicted by the simulation for each actuator was proven rational and realistic by the physical testing procedures. The FGM actuator showed a significantly higher output force (1.6 times more, with 137mN, at 2 psi) than the half-and-half actuator.

It also produced two times the displacement than the other actuator. The experimental values were mostly consistent with the predicted relationship.

Figure 5.14.: Final Gripper Assembly.

6. Discussion

This paper presents the results of the design, modeling, and fabrication of a soft silicone pneumatic actuator. It also includes the same for a layered, functionally graded version of the actuator, and a gripper assembly composed of three actuators symmetrically spaced about for grasping objects of choice, at about the same dimensions as a human hand. This offers the unique advantages of soft actuators instead of traditional rigid electromechanical actuation systems. The primary advantages of this soft actuator design are its simplicity, versatility, and scalability. The experimental part of this study focused on effective manufacturing of functionally graded silicone actuators. The design part of the study focused on finite element analysis according to tensile testing data for a linear distribution of elastic moduli against magnetite proportion. The design and materials were chosen for their economical budget and effective mechanical properties. The Ecoflex 0030 silicone proved efficient as a control in its pure form for its elastic properties that allowed smooth deformation as an actuator upon less than 5 psi of input pneumatic pressure.

6.1. Constraint Design

The actuator demonstrated different manners of deflection depending on the constraint type used. Systematic experimentation proved which design was best. The single-nylon-strand three-ring design proved ineffective, as the actuator inflated excessively and did not deflect more than a few millimeters. The two-strand helical constraint design increased the

degree of deflection but it did so in a non-uniform manner; silicone inflation along the length of the actuator was irregular. The optimal constraint design turned out to be the 10-ringed, single-strand form, with smooth deflection upon a range of input pressures.

6.2. Moisture Content

The moisture content that seeped into the paper holding the initial samples is a point that warrants consideration. The oils were not an expected result from leaving the samples out for a long duration (about 3 months), but their significance lies in the implication regarding the durability of the actuator. The polymer actuators are extremely durable, showing extremely desirable properties in terms of elastic deformation, and can be compressed or blown up to a relatively excessive extent without rupturing (despite their small dimensions). Aging silicone, however, is a point worth pursuing, as the actuators seemed to maintain their original properties after weeks in room temperature but the dogbone samples demonstrated a small degree of drying through seeping out their moisture content.

Silicone is generally considered very hydrophobic and nonpolar based on its relatively low surface energy and solubility parameter, along with its high contact angle with water (droplets maintain a spherical form on a silicone surface). Silicone typically only demonstrates hygroscopic (moisture-absorbing) properties with surface contaminants and in elastomers with bonds that easily re-orient towards the polar substrate. Compounds with more molecular mobility have a lower contact angle with water. Highly crosslinked polymers will demonstrate the opposite effect [23]. So, while silicone generally demonstrates hydrophobic properties, almost every polymer (besides polyolefins) exhibits some level of polarity and therefore can absorb some degree of moisture from the atmosphere. This is why at plastic processing plants, dryers are a standard piece of equipment [24]. Given this further research, it is worth considering more hydrophobic polymers if the moisture content proves to be a problem in long-term actuator durability. Polyolefin elastomers (or POEs) are a relatively

new class of polymers that provide superior elasticity, toughness, and low temperature ductility. They are viable in many flexible plastics applications and may be worth researching for their purely nonpolar chemical characteristic [25].

6.3. Experimental Error

The first round of tensile testing results for the 12% and 16% mixed polymer samples demonstrated data that was more spread out (poor precision) and unrealistic according to their higher stiffness (values were not as high as anticipated). Assuming experimental error, the team measured and observed the problematic samples. Potential sources of error were noted: magnetite settling (pouring the mixes too late–more than 10 minutes–could result in the particles settling down in the silicone due to gravity), inaccurate dimensions of the samples (at such a small scale, it was easy to pour a drop too little or too much upon casting, making the samples inconsistent), or an inaccurate amount of magnetite powder may have been added to the mix (the lab had two scales, one that measured grams to the tenths place, and another that measured to the hundredths place but fluctuated significantly during use, perhaps due to oversensitivity). These prove that it is necessary to be very careful with experimental procedures to get accurate and precise results. The team improved its methods throughout the duration of the project to attain the more accurate final results.

A direct comparison between the two FEA simulation results (for displacement and pressure) and the experimental data reveals that the simulations produce predictions that approximate the measured values that the actual gripper applies on a scale during experimentation. Abaqus proved to be a reliable program for prediction of dynamic response according to input mechanical properties. The approximate maximum force of the assembled gripper at full grasping form is 17g, and the simulation predicts 16.66g at 3psi. The results suggest that the elastic moduli derived from the tensile testing data were fairly accurate to the true mechanical properties of the elastomer. That being said, more tensile tests

with more samples would create more accurate data for a more accurate simulation.

The displacement values output by the half-and-half actuator simulation curiously predicted that the actuator would demonstrate further deflection than the FGM actuator. Testing resulted in the FGM actuator producing two times the displacement than the other actuator. The experimental FGM values were more or less in agreement with the simulated data, but the half-and-half testing demonstrated far less displacement than would be expected based on the simulated model. Despite this, considering the properties rationally, it makes sense for the FGM actuator to displace farther, given its functional design and its previous force output results. So, while the experimental data does not match the simulated output, it may be assumed that the FEA model was an imperfect representation of the deformation potentially due to missing or incorrect material parameters. There are a myriad of variables that go into describing a hyperelastic material's properties.

6.4. Directions for Future Improvements

Altogether, the data from the differing proportions of volume fractions in the samples as well as the manufactured actuators are in very good agreement with the experimental data. That being said, there is room for improvement in both the methods and the goals for this area of soft robotics. This study proved that as the material stiffness increases it demonstrates properties that cause actuator deflection according to appropriate design. However, one shortcoming is that it does not fully account for the range of designs that could be created with the methods used in this experiment. The team used a half-and-half and a layered design, but further research could experiment with more layering, layering in uneven proportions, or even something like a spiraled or double-helix casting, if possible through manufacturing methods.

This methodology for soft robot manufacturing demonstrates various advantages over many similar contemporary designs. Cable-driven actuators with attached motors are rel-

atively stiffer and heavier than fully soft ones. They also must deal with the challenge of designing secure attachments and interfaces between hard and soft components [22]. This project made use of a stopper-like 3D-printed fixture for securely connecting the pneumatic tubes to the silicone actuators without a high manufacturing cost. The Maker Movement and its associated democratization of manufacturing with personal 3D-printers has removed the hurdle of immediate capital investment, time, and aptitude to making a wide range of complicated hardware that previously necessitated expensive injection molding [6]. In order to make the system more portable, a smaller air tank with compressed air could be used in place of the 11-gallon one used for this project's prototype.

There are a many directions this project can take in the future. Potential steps for future progress include taking advantage of its versatility by developing more advanced actuators that can contort to a variety of geometries. Furthermore, the project's scalability can be explored by creating actuators of different dimensions, to see how this change might affect their function. This project only developed soft actuators that bend in one plane, but if a longer actuator was used with a different nanoparticle distribution it might be able to deflect in multiple directions. Also, using a spiral or helical pattern for the nanoparticle distribution could theoretically cause the actuator to twist along its cylindrical axis, for a more complex motion using a more complicated manufacturing method.

The project can also be expanded to include sensing capabilities. One of the most important benefits of soft robotics is the ability for the system to handle fragile or oddly-shaped objects. These capabilities are only enhanced when sensors are added. This can be accomplished by including air pockets along the actuator, attached to digital pressure sensors. Using this information, the central processing unit can tell whether or not the actuator is gripping an object or the amount of force needed to grip that object.

Aside from these manufacturing, design, and sensor opportunities for future improvement, this research could be furthered with succinct but meaningful mathematical descriptions of the blend of kinematics and intelligence that makes up soft robotics analysis. It is

difficult to model friction and contact with a soft robot's non-traditional interactions with its environment, although steps in this direction have been made [4]. Contrary to traditional rigid robotic systems, soft robots tend to deform themselves to their environment rather than cause a deformation. With the environment remaining unmoved, the soft robot may still impose a force on external bodies. This requires a non-traditional, more fluidic modeling system.

7. Conclusion

In this paper, an Abaqus model (designed according to experimental data) and a series of cured polymer mixes were used to study the mechanical properties of magnetic nanoparticle (MNP)-filled silicone as they relate to actuator design and further applications, largely in the biomedical industry. Incorporating these nanoparticles increased the stiffness of the material, and the manner in which they were cast demonstrated the behavior resulting from this type of design. Finite element analysis properly predicted the mechanical response from the actuator based off the experimental data and the program's appropriate modeling of the geometry and stiffness effects. The study demonstrated the linearly approximated correlation between volume fraction of filler particles and the Young's Modulus of the polymer material. A final mechatronic gripper system, controlled remotely by a remote gesture glove, was built for further applications and to demonstrate the utility in the design. Future project opportunities could involve larger, more complex, or more innovative designs.

Appendices

A. Graphs from Tensile Tests

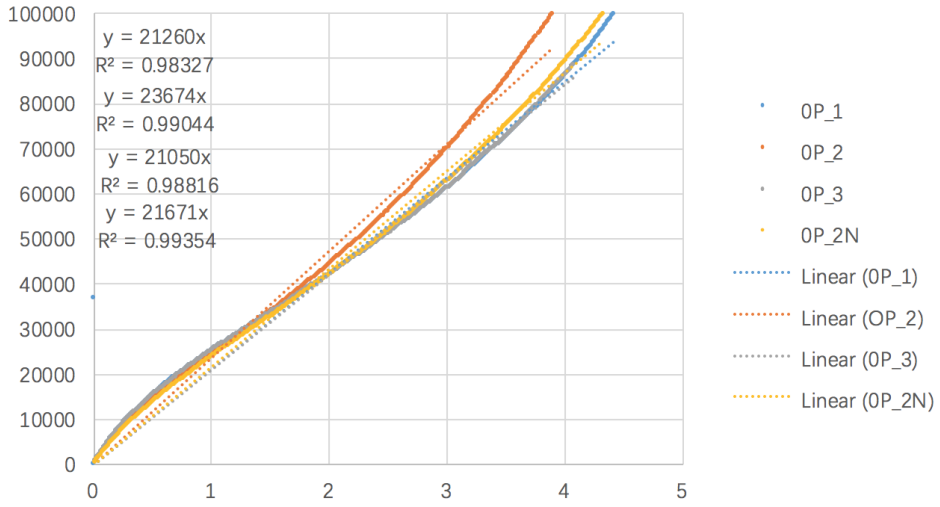

Figure A.1.: Tensile Test Results of 0% wt of Fe2O3 Specimens

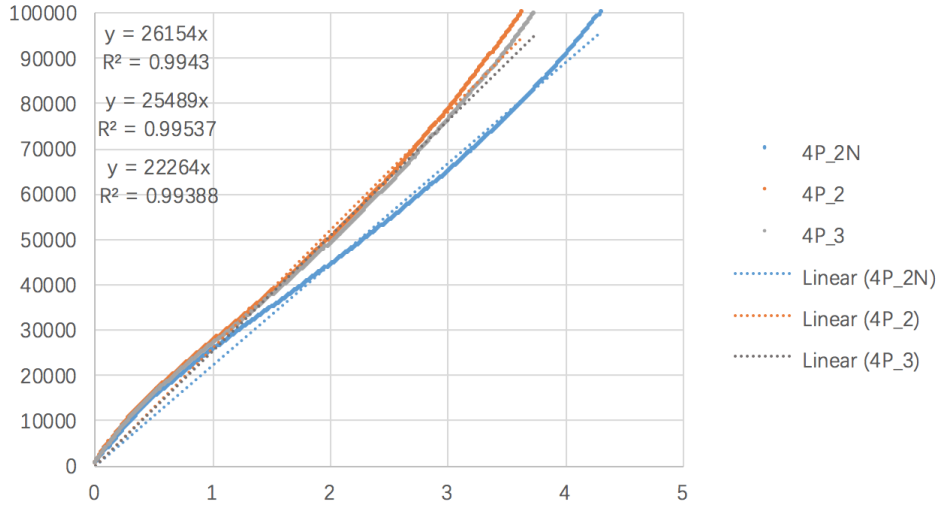

Figure A.2.: Tensile Test Results of 4% wt of Fe2O3 Specimens

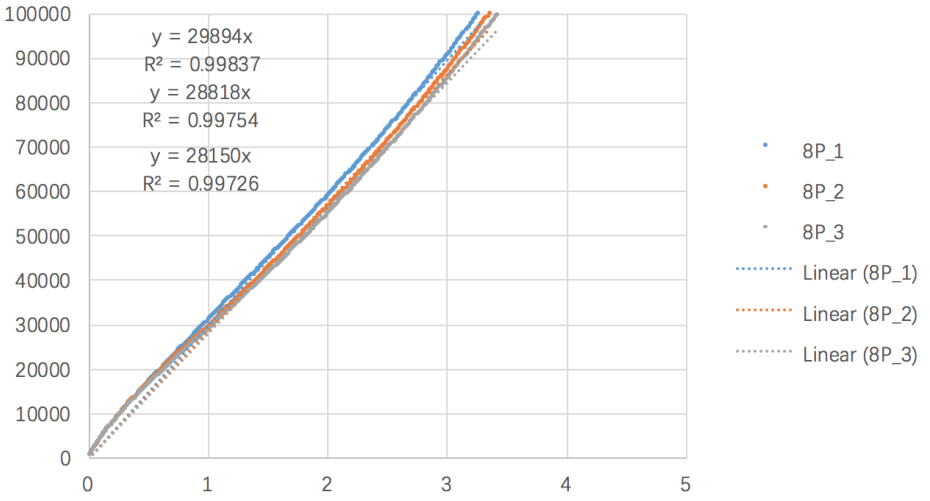

Figure A.3.: Tensile Test Results of 8% wt of Fe2O3 Specimens

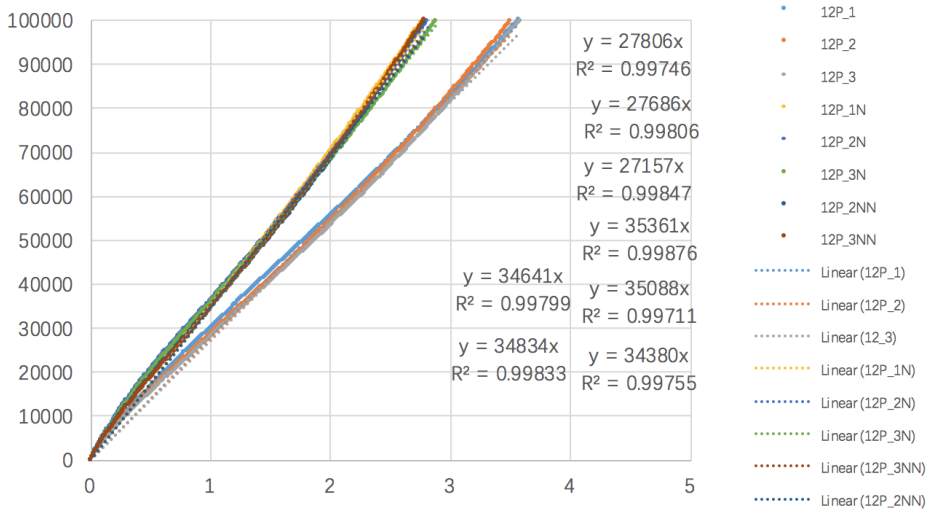

Figure A.4.: Tensile Test Results of 12% wt of Fe2O3 Specimens

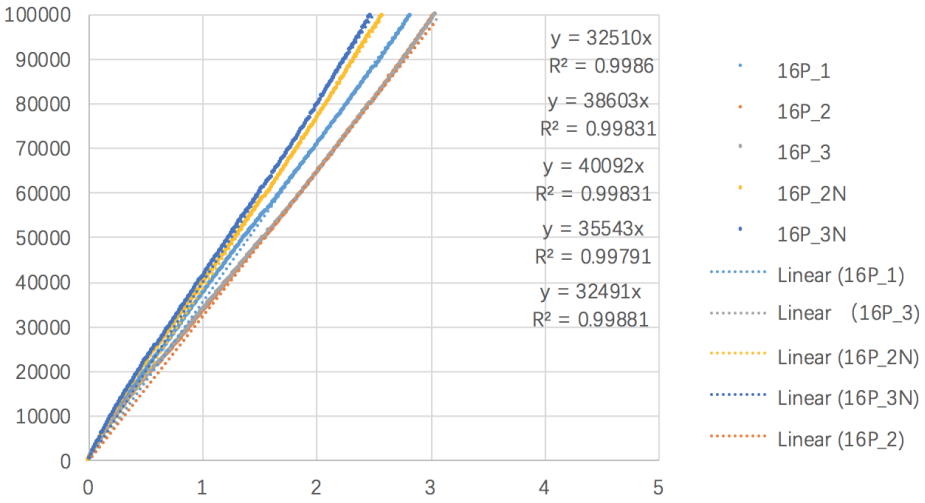

Figure A.5.: Tensile Test Results of 16% wt of Fe2O3 Specimens

B. Force and Deformation Tables

Pressure		Calculated Force		Experimental Force			Calculated Displacement		Experimental Displacement		Difference
Psi	kPa	mN	g-force	g-force	mN	% Difference	mm	in	in	mm	%
0	0.00	0.000	0.000				0	0			
0.5	3.45	29.143	2.972				14.0443	0.552925495			
1	6.89	58.295	5.944	7.267	71.262	22.243	28.0927	1.106012408	0.7	17.9	36.318
1.5	10.34	87.438	8.916	11.333	111.142	27.109	42.137	1.658937904	1.4	36.6	13.037
2	13.79	116.581	11.888	14.033	137.620	18.047	56.1813	2.211863399	2.8	72.1	28.293
2.5	17.24	145.733	14.861				70.2296	2.764946375			
3	20.68	174.876	17.832				84.2739	3.31787187			

Figure B.1.: Results of Force and Deformation for the FGM model

Pressure		Calculated Force		Actual Force			Displacement		Experimental Displacement		Difference
Psi	kPa	mN	g-force	g-force		% Difference	mm	in	in	mm	%
0	0.00	0.000	0.000				0	0			
0.5	3.45	27.225	2.776				17.9058	0.704953137			
1	6.89	54.459	5.553	5.933	58.186	6.845	35.8168	1.410110998	0.25	6.35	82.271
1.5	10.34	81.684	8.329	6.467	63.416	22.364	53.7226	2.115064134	0.65	16.51	69.268
2	13.79	108.909	11.106	8.933	87.606	19.560	71.6284	2.820017271	1.43	36.40666667	49.173
2.5	17.24	136.142	13.883				89.5394	3.525175132			
3	20.68	163.368	16.659				107.445	4.230120395			

Figure B.2.: Results of Force and Deformation for the Half-and-Half model

C. Engineering Drawing for the 3D-Printed Gripper Fixture

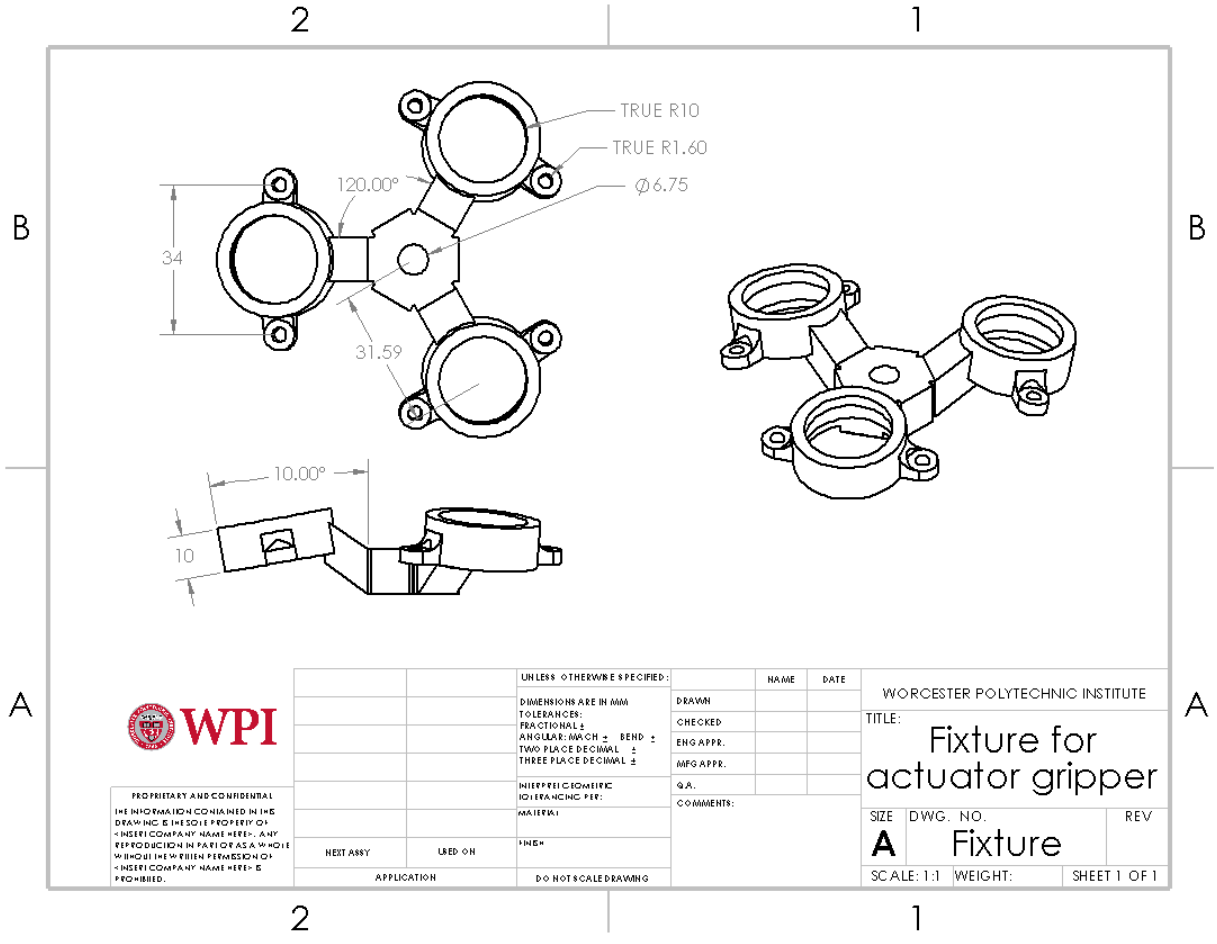

Figure C.1.: Engineering Drawing of Gripper Fixture

Bibliography

[1] Trivedi, D., Rahn, C. D., Kier, W. M., & Walker, I. D. (2008). Soft robotics: Biological inspiration, state of the art, and future research. Applied Bionics and Biomechanics, 5(3), 99-117.

[2] Zhang, Jiawei, et al. "A Modular, Reconfigurable Mold for a Soft Robotic Gripper Design Activity." Frontiers, Frontiers, 4 Sept. 2017, www.frontiersin.org/articles/10.3389/frobt.2017.00046/full. Accessed 28 Sept. 2017.

[3] Iida, Fumiya, and Cecilia Laschi. Soft Robotics: Challenges and Perspectives. 22 Dec. 2011, www.sciencedirect.com/science/article/pii/S1877050911006958. Accessed 10 Apr. 2018.

[4] "Soft Robotics." Soft Robotics, www.liebertpub.com/soro. Accessed 28 Sept. 2017.

[5] "Soft robotics: a bioinspired evolution in robotics." Trends in Biotechnology, Elsevier Current Trends, 12 Apr. 2013, www.sciencedirect.com/science/article/pii/S0167779913000632. Accessed 28 Sept. 2017.

[6] Schultz, Joshua, et al. "What Is the Path Ahead for Soft Robotics?" Soft Robotics, www.liebertpub.com/doi/10.1089/soro.2016.29010.jsc.

[7] Soft Robotics, www.softroboticsinc.com/use/.

[8] Suzumori, K., Iikura, S., & Tanaka, H. (1991). Development of flexible microactuator and its applications to robotic mechanisms. Proceedings. 1991 IEEE International Conference on Robotics and Automation,1622-1627. doi:10.1109/robot.1991.131850

[9] Kurumaya, Shunichi, et al. "Design of thin McKibben muscle and multifilament structure." ScienceDirect, Elsavier - Sensors and Actuators A: Physical, 1 July 2017, www.sciencedirect.com/science/article/pii/S0924424716308792. Accessed 28 Sept. 2017.

[10] Trimmer, Barry A. "Faculty & Research." Tufts University, Department of Biology: Faculty and Research, Tufts University, ase.tufts.edu/biology/faculty/trimmer/. Accessed 28 Sept. 2017.

[11] Kim, S., Laschi, C., & Trimmer, B. (2013). Soft robotics: A bioinspired evolution in robotics. Trends in Biotechnology,31(5), 287-294. doi:10.1016/j.tibtech.2013.03.002

[12] Trimmer, Barry A. "Current Research Projects." Tufts University: Neuromechanics and Biomimetics Devices Lab: Research, Tufts University, ase.tufts.edu/biology/labs/trimmer/research/.

[13] Laschi, Cecilia. "Soft Robotics." The BioRobotics Institute, Scuola Superiore S. Anna, sssa.bioroboticsinstitute.it/research/softrobotics. Accessed 28 Sept. 2017.

[14] Cianchetti, Matteo. "Octopus Integrating Project." Octopus Integrating Project, Octopus Partnership, www.octopusproject.eu/. Accessed 28 Sept. 2017.

[15] Menciassi, Arianna. "Surgical Robotics and Allied Technologies." Surgical Robotics and Allied Technologies — The BioRobotics Institute, Scuola Superiore S.Anna, sssa.bioroboticsinstitute.it/research/surgicalrobotics.

[16] Onal, C. and Sun, Y. (2018). Ecoflex Material Properties. Worcester Polytechnic Institute.

[17] Solid and Liquid Silicone Rubber Material and Processing Guidelines. Solid and Liquid Silicone Rubber Material and Processing Guidelines, Wacker Chemie AG, 2015.

[18] Luo, Ming, et al. "Modeling, Integration, and Control of Reverse Pneumatic Artificial Muscles (rPAMs)." IEEE Transactions On Robotics.

[19] Kan-Dapaah, K., Rahbar, N., Tahlil, A., Crosson, D., Yao, N. and Soboyejo, W. (2015). Mechanical and hyperthermic properties of magnetic nanocomposites for biomedical applications. Journal of the Mechanical Behavior of Biomedical Materials, 49, pp.118-128.

[20] Iron Oxide Nanopowder / Nanoparticles (Fe2O3, 2. (2018). Iron Oxide Nanopowder / Nanoparticles (Fe2O3, gamma, high purity, 99.5+%, 20 nm). [online] Us-nano.com. Available at: http://www.us-nano.com/inc/sdetail/233 [Accessed 5 Mar. 2018].

[21] Smooth-On, Inc. (2018). Silc Pig® Product Information. [online] Available at: https://www.smooth-on.com/products/silc-pig/ [Accessed 5 Mar. 2018].

[22] Trimmer, B. (2017). A Practical Approach to Soft Actuation. Soft Robotics, 4(1), 1-2. doi:10.1089/soro.2017.29011.bat

[23] M.J. Hunter et al., Ind. Eng. Chem, 1947, 39, 1389

[24] Sepe, M. (2014, April 24). Why (and What) You Need to Dry. Retrieved from https://www.ptonline.com/articles/why-and-what-you-need-to-dry

[25] AZoM, W. B. (2017, August 01). Polyolefin Elastomers - Properties and Applications of Polyolefin Elastomers (POE). Retrieved from https://www.azom.com/article.aspx?ArticleID=1959

[26] Onal, C., Chen, X., Whitesides, G., & Rus, D. (2017). Soft mobile robots with on-board chemical pressure generation. Retrieved from https://pdfs.semanticscholar.org/a454/515b643733db71d02c5b2c9e2bb72379c0e0.pdf